Numerical Analysis of Novel Savonius type Hydrokinetic Turbine

Author

Zain Ullah Khan

Registration Number

00000275632

Supervisor

Dr. Zaib Ali

DEPARTMENT OF MECHANICAL ENGINEERING

SCHOOL OF MECHANICAL & MANUFACTURING ENGINEERING

NATIONAL UNIVERSITY OF SCIENCES AND TECHNOLOGY

ISLAMABAD

SEPTEMBER, 2020

Numerical Analysis of Novel Savonius type Hydrokinetic Turbine.

Author

Zain Ullah Khan

Registration Number

00000275632

A thesis submitted in partial fulfillment of the requirements for the degree of

MS Mechanical Engineering

Thesis Supervisor:

Dr. Zaib Ali

Thesis Supervisor's Signature: _____

DEPARTMENT OF MECHANICAL ENGINEERING

SCHOOL OF MECHANICAL & MANUFACTURING ENGINEERING

NATIONAL UNIVERSITY OF SCIENCES AND TECHNOLOGY,

ISLAMABAD

SEPTEMBER, 2020

THESIS ACCEPTANCE CERTIFICATE

Certified that final copy of MS thesis written by Mr. **Zain Ullah Khan** Registration No. **00000275632** of **SMME** has been vetted by undersigned, found complete in all aspects as per NUST Statutes/Regulations, is free of plagiarism, errors, and mistakes and is accepted as partial fulfillment for award of MS/MPhil degree. It is further certified that necessary amendments as pointed out by GEC members of the scholar have also been incorporated in the said thesis.

Signature with stamp: _____

Name of Supervisor: Dr. Zaib Ali

Date: _____

Signature of HoD with stamp: _____

Date: _____

Countersign by

Signature (Dean/Principal): _____

Date: _____

Declaration

I certify that this research work titled "*Numerical Analysis of Novel Savonius type Hydrokinetic Turbine"* is my own work. The work has not been presented elsewhere for assessment. The material that has been used from other sources it has been properly acknowledged / referred.

Signature of Student

Zain Ullah Khan

2018-NUST-MS-Mech-00000275632

Plagiarism Certificate (Turnitin Report)

This thesis has been checked for Plagiarism. Turnitin report endorsed by Supervisor is attached.

Signature of Student

Zain Ullah Khan

Registration Number

MS-ME-00000275632

Signature of Supervisor

Copyright Statement

- Copyright in text of this thesis rests with the student author. Copies (by any process) either in full, or of extracts, may be made only in accordance with instructions given by the author and lodged in the Library of NUST School of Mechanical & Manufacturing Engineering (SMME). Details may be obtained by the Librarian. This page must form part of any such copies made. Further copies (by any process) may not be made without the permission (in writing) of the author.
- The ownership of any intellectual property rights which may be described in this thesis is vested in NUST School of Mechanical & Manufacturing Engineering, subject to any prior agreement to the contrary, and may not be made available for use by third parties without the written permission of the SMME, which will prescribe the terms and conditions of any such agreement.
- Further information on the conditions under which disclosures and exploitation may take place is available from the Library of NUST School of Mechanical & Manufacturing Engineering, Islamabad.

Acknowledgements

I am thankful to my Creator Allah Subhana-Watala to have guided me throughout this work at every step and for every new thought which You setup in my mind to improve it. Indeed I could have done nothing without Your priceless help and guidance. Whosoever helped me throughout the course of my thesis, whether my parents or any other individual was Your will, so indeed none be worthy of praise but You.

I am profusely thankful to my beloved parents who raised me when I was not capable of walking and continued to support me throughout in every department of my life.

I would also like to express special thanks to my supervisor Dr. Zaib Ali for his help throughout my thesis and also for CFD course which he has taught me. I can safely say that I haven't learned any other engineering subject in such depth than the ones which he has taught.

I would also like to pay special thanks to Dr. Emad Uddin for his tremendous support and cooperation. Each time I got stuck in something, he came up with the solution. Without his help I wouldn't have been able to complete my thesis. I appreciate his patience and guidance throughout the whole thesis.

I would also like to thank Dr. Zaib Ali, Dr. Muhammad Sajid and Dr. Emad Uddin for being on my thesis guidance and evaluation committee and express my special thanks to them for their support and guidance.

Finally, I would like to express my gratitude to all the individuals who have rendered valuable assistance to my study.

Dedicated to my exceptional parents and adored siblings whose tremendous support and cooperation led me to this wonderful accomplishment.

Abstract

Small-scale renewable power systems have gained attention in the past few years because of climate change, increased urbanization, global warming, excessive use of fossil fuels and high transmission costs. The push for a greater share of renewable energy in the overall energy mix is of more significance to Pakistan due to the chronic power shortfall and huge oil import bill. Some of the renewable energy resources often use these days are biomass, wind, hydro, solar and geothermal. Hydropower is the most abundant (water covering 71% of the planet) and economical source of renewable energy. Generally, there are two ways to harness energy from water, one is the hydrostatic approach which uses the potential head of flow and the other is a hydrokinetic approach that uses the kinetic energy of incoming flow to rotate the turbine. The conventional hydrostatic method requires the development of grandiose structure and construction of dams or reservoirs for power generation, storage and transfer. In contrast, hydrokinetic turbines require less or no civil work. Among hydrokinetic turbines, savonius type hydrokinetic turbine is environment friendly, simple and low cost power generation device for low speed flows. On the other hand, savonius hydrokinetic turbines have less power coefficient and torque than other hydrokinetic turbines. In this study, a novel Savonius type low speed hydrokinetic turbine has been proposed after careful analysis of torque and power coefficient at Tip Speed Ratio (TSR) range from 0 to 1.2. The proposed design comprises of S1048 section profile of diameter 0.33m having 14% more power coefficient than conventional savonius rotor. The S1048 section profile is utilized first time to design the blades of savonius hydrokinetic turbine using novel airfoil sectioning procedure. Transient CFD analysis has been carried out to obtain performance and torque coefficients. The numerical study has been carried out using finite volume method and RANS code with an inlet water velocity of 0.38m/s. *K*-ω SST turbulence model has been used to resolve turbulence effects. In addition to that, an existing augmentation system comprising of curtain arrangement has been used with S1048 section rotor to further increase the turbine efficiency. The maximum power coefficient has been found equal to 0.43 at TSR of 1 using curtain plate augmentation system. The proposed turbine is in good agreement with validation model and is feasible for experimental testing and can harness power from low speed and low head water flows.

Key Words: HKT, CFD, Savonius HKT, S1048 section rotor, Turbine augmentation

Table of Contents

List of Figures

List of Tables

CHAPTER 1: INTRODUCTION

1.1 Background, Scope and Motivation

Conventional energy sources such as natural gas, coal and oil have proven to be extremely efficient for energy needs but on the other hand, they are having adverse effects on human health and environment. With the passage of time, conventional sources of energy are decreasing, and the world is looking towards renewable energy resources to fulfill energy demands. The world energy consumption will raise by 56% from 2010 to 2040. As world population continues to increase and the limited amount of fossil fuels starts to reduce, there is an increasing demand to exploit renewable sources of energy according to the U.S. Energy Information Administration (USEIA). So the energy source should be renewable and should have fewer effects on ecosystem and environment. Renewable energy sources have significant environmental benefits over conventional sources [1].

Turbomachine is a device in which the energy is transferred either to or from a continuously flowing fluid by the dynamic action of one or more moving blade rows. It plays a major role in particular in aircraft, marine space (liquid rockets), land propulsion systems but also in hydraulic, gas and steam turbines applications. It is also involved in industrial pipeline and processing equipment such as gas, petroleum and water pumping plants. Other applications can be related to heart-assist pumps, industrial compressors and refrigeration plants, among others. The turbo machinery field includes turbines, pumps, fans, compressors. The turbomachine which we have chosen for our analysis is a hydrokinetic turbine whose principle is to extract energy from the fluid and convert it into mechanical energy as power output at the shaft.

1.2 Characteristic and trends in Hydrokinetic Turbines

Some of the renewable energy resources often use these days are biomass, wind, hydro, solar and geothermal. Hydropower is the most abundant (covering 75% of the planet) and economical source of renewable energy. It is also the most effective method to produce electricity. There are primarily two procedures to harness water energy that are hydrostatic and hydrokinetic methods. The hydrostatic approach is the conventional way to harness energy from water which uses the potential head to generate energy. This method requires development of grandiose

structure and construction of dams or reservoirs for power generation, storage and transfer. Moreover, conventional micro-hydro usually have high primary capital cost and less running costs [2]. On the other hand, hydrokinetic systems use the kinetic energy of water to drive rotor for power generation. It requires less or no civil work. Hydrokinetic turbines working principle is same as wind turbines. Water destiny is approximately 800 times more than air so hydrokinetic turbines can generate enough power at low speed. It can operate at a low speed of water typically from 0.5m/s and above [3]. The term 'Hydrokinetic Turbine' is also known as, 'Zero Head hydro Turbine', 'Free Flow or Stream Turbine', 'Water Current Turbine' (WCT), 'In-stream Hydro Turbine', or 'Ultra-low-head Hydro Turbine' [4]. The main regions where hydrokinetic turbines can be installed are tidal current, ocean currents, irrigation and other manmade canals [4,5]. Hydrokinetic turbines are commonly divided into horizontal axis, vertical axis and cross flow turbine according to the direction of flow with respect to rotation of shaft [4].

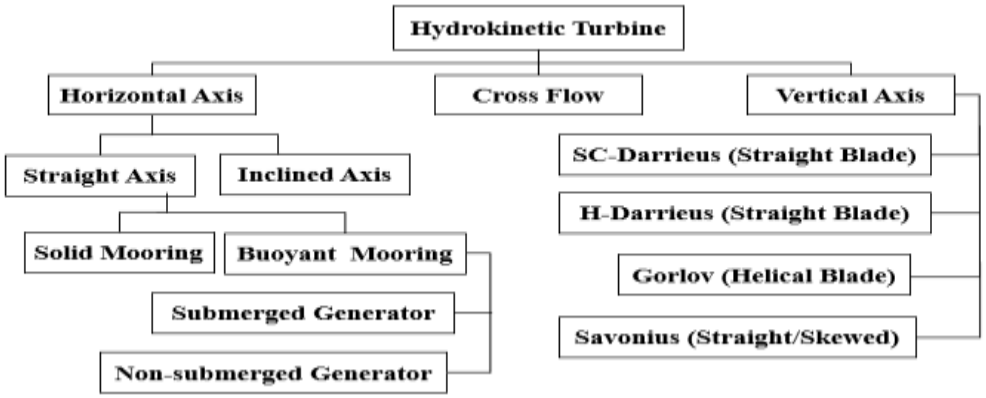

Figure 1.1: Classification of Hydrokinetic turbines

The physical arrangements of different types of HK turbines are shown below in Figure 1.2.

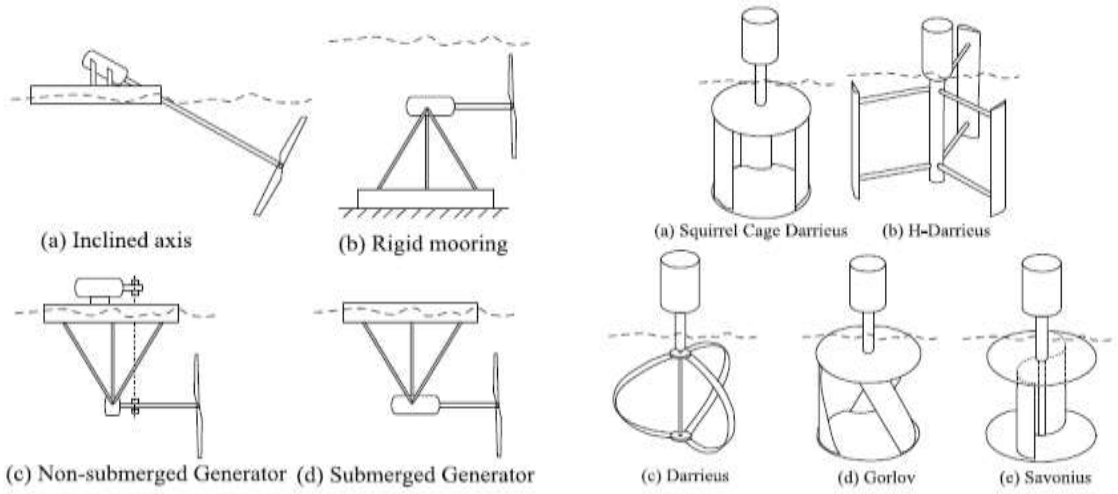

Figure 1.2: Horizontal and Vertical Axis HK turbines [4]

1.2.1 Advantages and Disadvantages of Horizontal and vertical axis Hydrokinetic Turbines

Some of the advantages and disadvantages of both types of hydrokinetic turbines are listed below in table 1-1.

Table 1-1: Pros and Cons of vertical and horizontal axis HK turbines [3][4][5][6][7].

Turbine configuration	Advantages	Disadvantages
Vertical axis turbines	➢ Design potentially simpler and less expensive. ➢ Low generator coupling costs due to placement above water. ➢ The cylindrical shape of turbines allows convenient mounting of various curvilinear or rectilinear ducts. These channels can also be employed for mooring and floating purposes. ➢ Vertical turbines generally emit less noise than the horizontal turbine concepts due to reduced blade tip losses. ➢ Can rotate unidirectional even with bi-directional fluid flow. ➢ More suitable for operation under shallow channel with varying water velocity and shallow stream with limited water flow rate. ➢ The cylindrical rotor shape makes cross flow turbines particularly suitable for small, low power riverine hydrokinetic applications. Alternative Hydro Solution Ltd. claims cross flow turbines are better than axial flow turbines in small and medium hydrokinetic applications. ➢ Deploy as a single unit in small rivers and stacked together to deploy in bigger rivers.	➢ Vertical axis turbines have low starting torque, torque ripple, and lower efficiency. ➢ Cavitation and fatigue loading due to unsteady hydrodynamics are other concerning issues associated with vertical turbines.
Horizontal axis turbines	➢ Self-starting capability and high efficiency. ➢ Annular ring type augmentation channels provide greater augmentation of fluid velocity as these systems allow concentrated/diffused flow in a three-dimensional manner. ➢ Optimum performance is achieved at higher rotor speed (marine/tidal conversion), this ease with the reduction of a reduced gear coupling. ➢ Active control by blade pitching allows greater flexibility in over-speed protection and efficient operation.	➢ High generator coupling cost due to underwater placement. ➢ Clogged with debris found in rivers. ➢ Very costly in manufacturing and maintenance. ➢ Only as a single unit due to disc-shaped rotor and impossible to deploy in small, narrow river.

Axial flow turbines are generally used for tidal and ocean applications, probably because of their high-efficiency [4,5,6]. Cross flow turbines can have diameter larger than depth which allows them to sweep a bigger area in shallow river streams, increasing the possible power production per turbine [6]. Hence the vertical axis Savonius HK turbine is selected for this research.

1.2.2 Augmentation Techniques used in Hydrokinetic Turbines

Augmentation techniques are also used in hydrokinetic turbines to increase the flow velocity and sometimes to concentrate flow around the turbine blades. Thus the power output increases. The types and shapes of some augmentation devices are shown below in Figure 1.3.

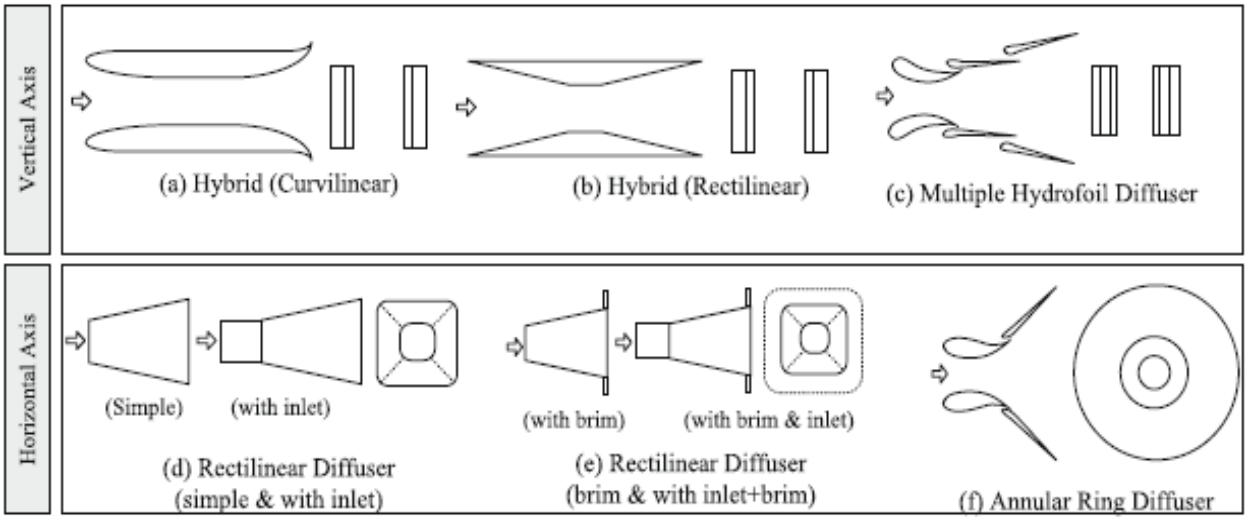

Figure 1.3: Augmentation channels shapes [4].

Hydrokinetic energy systems face various challenges depending upon the turbine configuration and flow parameters inside the river. Some challenges arise when trying to utilize vertical axis hydrokinetic turbine in a river for potential assessment, these challenges include, low water speed not sufficient for the turbine, less performance of savonius hydrokinetic turbine, structure reliability and stability, spatial and temporal flow properties of river with river cross section and depth, and effective operation and control designed for optimization of system performance. Therefore for a hydrokinetic turbine to successfully operate on the river site, these challenges must be resolved to an acceptable level. In the present study, we will address the first two challenges i.e. low water speed and low efficiency of savonius hydrokinetic turbine. A novel blade design is proposed in the present study to increase the hydrodynamic efficiency of savonius

hydrokinetic turbine. Furthermore, an experimentally optimized curtain plate augmenter [7] is combined with the rotor to enhance the performance of savonius hydrokinetic turbine. This augmenter is used to increase the speed of the water near the rotor blades.

1.3 Organization of thesis:

This thesis is divided into five chapters. The first chapter consists of two sections, the first section presents the background and trends in hydrokinetic energy systems. While the second section discusses the basics of two bucket Savonius turbine and literature review related to the performance of savonius rotor. Finally, this chapter presents the research questions.

The second chapter elaborates the studies already done on the Savonius turbine. In particular, the chapter highlights the research development in the field of the savonius turbine, presenting both experimental and simulation studies. In this chapter, the impact of various arrangements is reviewed and presented. The third chapter discusses the numerical modeling. Moreover, it includes turbulence modeling, governing equations, mesh generation, and simulation procedure. Validation and convergence studies are also included in this chapter. The fourth chapter presents the results and extensive discussion of simulation results. This chapter has two main parts. The first part includes the discussion between a conventional rotor and a newly proposed S1048 airfoil rotor. While the second part focuses on the discussion related to the augmentation system. Lastly, the final chapter gives a conclusion about the thesis, highlighting the findings of this research and presenting suggestions and further studies prospects.

CHAPTER 2: LITERATURE REVEIW

2.1 SAVONIUS HYDROKINETIC TRUBINE

Savonius rotor is a 'S' type rotor made up of two semi-circular blades having a slight overlap distance between blades as shown below in Figure 2.1. With better starting characteristics, Savonius rotor has the ability to receive fluid from almost any direction. However, it has less aerodynamic efficiency as compared to darrieus rotor.

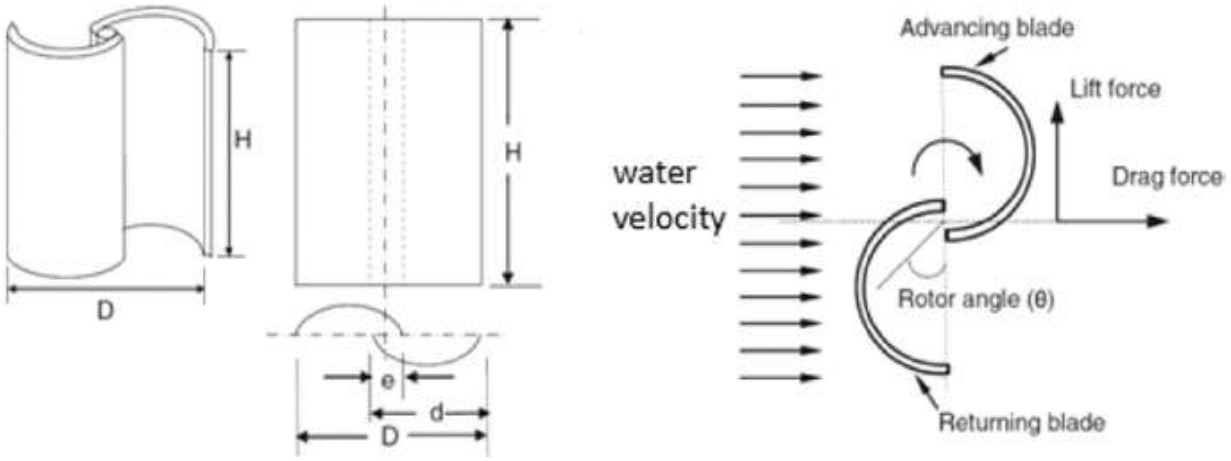

Figure 2.1: A Typical two blade savionus rotor [9].

In the above Figure, 'H' is the representation of the height of the rotor whereas the diameter of the rotor is denoted by 'D'. The ratio between these two dimensional quantities i.e. 'H' and 'D' is coined as 'The aspect ratio'. There is an additional parameter upon which the coefficient of power of savonius rotor depends and it is named as 'the overlap ratio' (β) which is normally represented in the form of $\beta = e/d$, here d is the diameter of the blade and e is the overlap distance. Upon impingement of the free force, the advancing blade creates a drag force on the other hand the returning blade generates a returning force from the flow through the overlapping gap that is in opposing direction creating a pair of couple forces from which we get the generated torque and power.

2.1.1 Design Parameters

Savonius hydrokinetic turbine parameters are similar to Savonius wind rotor. That are aspect ratio, Overlap ratio, Gap ratio, Endplate, Blade shape, Rotor angle, Multi-staging, Number

of blades, Tip speed ratio and Reynolds Number. These are the major parameters that affects the performance of savonius rotor. In the later sections, we will discuss the effect of these parameters on the efficiency of the turbine investigated by different researchers.

2.2 Aspect ratio effect on performance:

Aspect ratio (AR) is an important parameter which effects the performance of the turbine. It is usually represented as AR=H/D here H is blade height and D is turbine diameter. Many researchers studied the effect of aspect ratio on *Cp* of savonius rotor. In review paper [8], the ranges of aspect ratio used up till know are elaborated. In case of two blades semicircular savonius rotor, it is suggested that aspect ratio of 4.8 shows the best *Cp* of 0.243. While for a modified rotor without shaft, the maximum Cp is found at the aspect ratio of 0.7 [8].

2.3 End plate effect on performance:

End plate affects the performance of the turbine because of fluid leakage and flow physics. Jeon [8] studied the influence of end plates on *Cp* of helical savonius rotor. He [8] concluded that larger area of end plate results in larger *Cp* of helical savonius rotor. Sivasegaram [9] also studied the influence of end plates on the performance of rotor. He [9] found the optimal end plate diameter that is equal to 1.1D (D = rotor diameter). A lot of researchers found that by using greater diameter rotor results in greater rotor inertia [10].

2.4 Overlap ratio effect on performance:

The overlap ratio is the ratio of blades overlapped length to the diameter of a blade. In order to increase the *Cp* (power coefficient) of savonius rotor, sometimes overlap ratio is important. Many researchers worked for the optimal value of the overlap ratio.

From the literature review, Kumar [10] concluded that for best performance, the overlap ratio should be from 0.15 to 0.25.

2.5 Number of blades effect on performance:

Number of blades generally effects the performance of hydrokinetic turbines. In savonius rotor mostly 2 blades are found optimal by most of the researchers. Mahmoud [11] studied the effects of the number of blades on savonius wind rotor with zero aspect ratio. He [11] found that

two blades turbine shows better performance over three and four blade rotors. Sheldahl [12] tested two and three blade savonius rotor experimentally. The overlap ratio and aspect ratio of his [12] turbine were 0.15 and 0.1 respectively. He [12] found that two blade rotor shows better *Cp* than three blade rotor. He got the maximum value of *Cp* of 0.24. Two bladed rotor has best *Cp* of 0.31 at the aspect ratio of 1.58 [8].

2.6 Multi-staging effect on performance:

Combining of single stage rotors one over another is known as multi-staging. It affects the performance of the rotor. Mahmoud [10] studied the stages effects on savonius rotor. He [10] found that two stage rotor performs better than a single stage. As reported by [8], two stage turbine has a maximum *Cp* above 0.3. From the review paper [8], he concluded that 1 and 2 stage rotor are optimum for better *Cp*.

2.7 Blade Profile effect on performance:

Savonius rotor blade profile is an important parameter which effects the rotor performance. A lot of researchers worked on 2D and 3D profiles with a twist in order to maximize *Cp* of the rotor. Roy and Saha [13] tested experimentally four different types of blade profiles for 2 blade savonius rotor and deployed there new modified model.

The newly developed model shows higher *Cp* followed by modified bach type, Benesh type, semi-elliptical and conventional SSWT. The maximum *Cp* of the newly developed model was 0.31 [13].

The summary of airfoil type 2D blades are reported by [14]. The review paper [14] shows that the S-section profile has a maximum *Cp* of 0.37 in experimental testing. Blade profiles and shapes developed up till now is shown below.

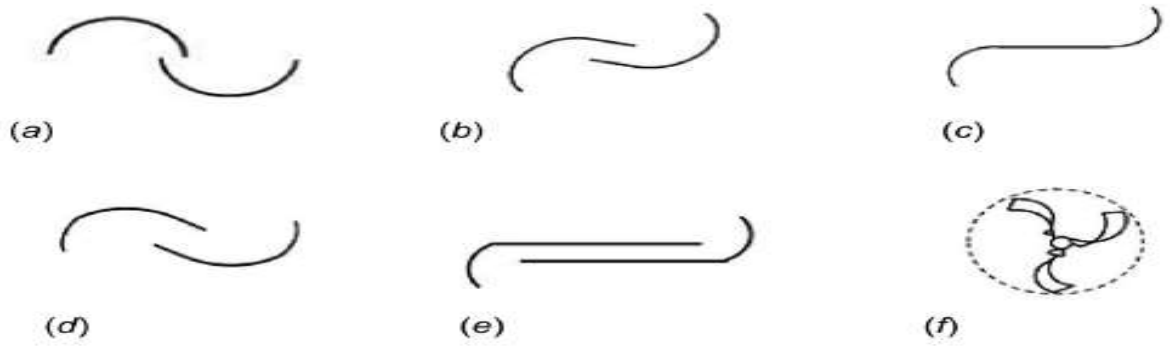

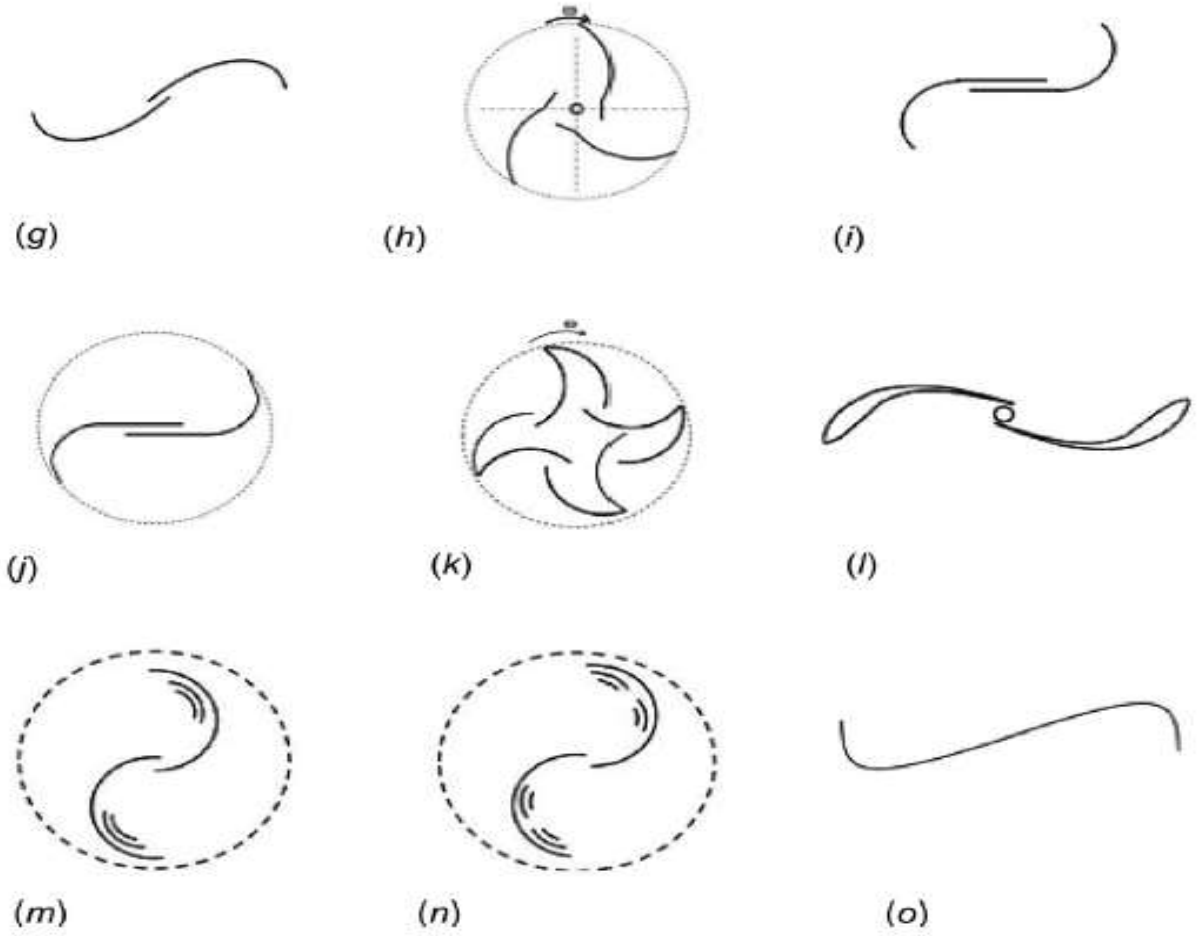

Evolution of Blade profiles for Savonius rotors:- (a) [1929] semicircular, (b) [1930] semicircular, (c) [1931] Bach, (d) [1988] Benesh, (e) [1996] Benesh, (f) [2004] Twisted, (g) [2013] Elliptical, (h) [2013] Fish ridged rotor, (i) [2014] Modified Bach profile, (j) [2014] Roy profile, (k) [2014] Bronzinus, (l) [2015] Airfoil shape profile, [m] (2016) Multiple quarter semicircular, (n) [2017] Multiple miniature semicircular, and (o) [2017] Spline profile [13].

Elliptical profile *Cp* is maximum among the profiles shown above which is 0.33 followed by Roy [13] newly developed profile whose *Cp* is 0.31 [15].

Saha [15] conducted a review that how different augmentation procedures affect the performance of savonius rotor. Savonius rotor with guide vanes has a maximum *Cp* of 0.52 [15].

3D blade profiles with angle of twist are also investigated by many researches in wind rotors. At the different angle of twist different researchers investigated the rotor. CFD analysis shows that at a helical angle of 45 degrees, *Cp* of the rotor was maximum which is about 0.462 at

TSR 1.63[14].

2.8 Savonius Rotor Augmentation methods:

Savonius rotor is a drag type turbine. Due to this fact its coefficient of power is lesser than lift type darrieus vertical axis turbines. Researchers have developed many techniques to increase the performance of the rotor using augmentation. Actually, there is two common purposes for using augmenter. First, to increase the flow velocity. Second, to concentrate the flow around the advancing blade rather than both blades because the returning blade generates negative torque which reduces the performance.

The summary of different augmentation techniques used for performance enhancement is presented in the review paper [15].

Among the augmenters presented in the review paper [15], the guide vane shows a maximum power coefficient of 0.52. However, the design of guide vane is complex and it requires more manufacturing cost. Another augmenter with a shield has a maximum coefficient of performance of 0.50. But this design was adopted with six blade savonius rotor. Hence for the present study the curtain plates design is selected for performance enhancement. [7]. The curtain design contains two straight plates. Moreover, curtain design is easy to fabricate. The coefficient of performance of three different configurations of curtain design is shown below.

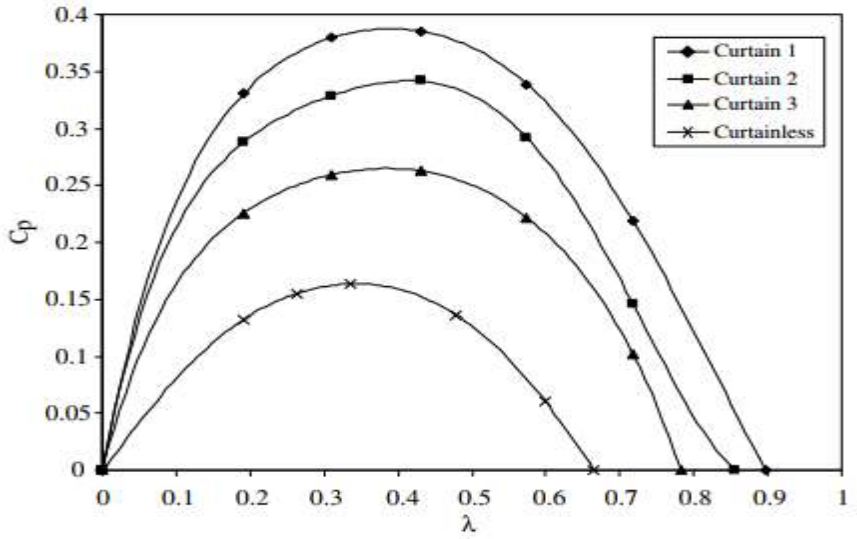

Performance comparison of different curtain lengths [7]

All curtain designs show a rise in the power coefficient. But the curtain design 1 shows the best

performance for wider ranges of TSR. This arrangement has the ability to collect more flow and deflect flow appropriately.

2.9 Research studies associated with Savonius HKT:

Research studies on the performance of savonius hydrokinetic turbines are shown in Table 2-1.

Table 2-1: Evolution in SHKT

Authors	**Methodology**	**Blade shape**	**C_{Pmax} & (Turbine Parameters)**	**Additional Features Investigated**
Nakajima (2008)[16]	Experimental	Semicircular SHT	0.25 (β 0.36, Re 1.1×10^5)	Visually Examined flow field around rotor. Studied the effect of installation parameters.
Khan (2009)[17]	Experimental	Semicircular SHT	0.038 for single stage 0.049 for double stage 0.04 for three stage	Investigated the effect of torque variation in single, double and three stage rotor.
Golecha K (2012)[18]	Experimental	Modified Savonius water turbine	0.35 with deflector 0.15 without deflector	Studied different positions of deflector plate and its impact on performance of rotor
Patel (2016)[19]	Experimental	Semicircular SHT	0.20 (β=0.13, AR =1.096)	Examined the effect of OR, AR and vanes.
Yaakob(2012)[20]	CFD (k-ε)	Semicircular SHT	0.275 (AR 1.1)	Simulated full scale model of H=7.5m and D=6.5m at flow speed of 0.56m/s.

Sarma(2014)[21]	Experimental and CFD (k-ε)	Three blade SHT	0.39 (AR=0.65)	Evaluated turbine at low water velocities of 0.3-0.9m/s. Performance of SHKT is better than Savonius Wind rotor.
Kumar (2017)[22]	CFD (k-ε realizable)	SHT with twisted blades	0.35 (Twist angle of 12.5°. AR =1.58)	Studied the effect of twist angle ranging from 0 to 25º while the flow velocity of water 0.5m/s to 2m/s.
Ahmed (2017)[23]	CFD (k-ω SST)	Modified Savonius Water turbine	0.25 (Re 1.32×10^5)	Investigated six different novel configurations of duct nozzle system. Studied flow characteristics and effect of vertical and horizontal duct on performance of rotor.
Saha (2018)[24]	Experimental and CFD (*k*-ω SST)	Semicircular SHT Elliptical SHT	0.28 (Re=2.25×10^5) 0.17 (Re=2.25×10^5) (AR=1.0, β=0.15)	Investigated the effect of blade shape, no of blades and immersion level at water speed of 0.8m/s.
Mabrouk (2019)[25]	Experimental and CFD (*k*-ε realizable)	Three blade helical SHT	0.125 (Blade twist angle 90°. Blade Chord 90mm). (Optimal deflection angle 30°).	Studied and examined optimal configuration of new deflector system using NACA 0020 airfoil at flow velocity of 0.86m/s.
Hossein Alizadeh (2020) [26]	CFD (SST transition model)	Conventional Semicircular	18% increase in power coefficient (D=0.9, β=0.15)	Optimized circular barrier placed in upstream of the rotor. (Used nine sectors of barrier)

Savonius rotor is the most cost-effective and easily manufactured turbine among vertical axis

hydrokinetic turbines. In past years, a lot of research has been conducted to enhance the efficiency of savonius turbines. These studies include, numerical and experimental work, concentrated on optimizing blade profiles, optimizing geometric parameters and the use of different augmentation methods. As elaborated above, most of the work focused on 2D blade profiles and augmentation techniques to increase rotor performance. Two-dimensional blade profiles generally include conventional semicircular blade design. However, in recent years elliptical and modified blade profiles have been used. In present study, the section of S1048 airfoil is used for performance improvement. There are two main purposes of using this blade profile. Firstly the center of pressure of proposed profile is away from the center of rotation. Secondly, the extra overlap space between S1048 section blades increases the pressure on the convex side of the returning blade.

Some of the problems and challenges of savonius hydrokinetic turbines are discussed in the previous chapter. One of the challenges that we are addressing in the present work is the improvement of turbine performance using novel blade design. The second challenge is how to increase the speed of flow while entering the turbine domain. To resolve this problem, a curtain plate augmentation system is selected. In savonius wind turbines, a lot of blade profiles and augmentation methods have been tested both numerically and experimentally. But for savonius hydrokinetic turbines, up till now, very few models are tested. Therefore a novel blade has been designed and analyzed in the present study with a previous existing superior augmentation system.

CHAPTER 3: NUMERICAL METHODS AND MODELLING

The hydrokinetic turbine operates in water flow experiences turbulence effects. The flow around the rotor is assumed turbulent, unsteady and incompressible. In order to solve this flow problem accurately, first we will derive Reynolds Averaged Navier-Stokes. Through the extension of RANS, 2D simulation is carried out using transient analysis. RANS splits the flow velocity into two separate parts: a time average u and fluctuating u′.

$$\boldsymbol{u_i = u_i + u'_i}$$

U is the variable of velocity which changes both in space and time.

The derivation begins with the conservation of mass and momentum for incompressible flows.

$$\frac{\partial u_i}{\partial x_i} = 0 \tag{3.1}$$

$$\rho \frac{\partial u_i}{\partial t} + u_j \frac{\partial u_i}{\partial x_j} = -\frac{\partial p}{\partial x_i} + \frac{\partial t_{ij}}{\partial x_j} \tag{3.2}$$

Where ρ= density of water and t = stress tensor.

The stress tensor term in the above equation (2.2) can be extended as [27].

$$t_{ij} = 2\mu s_{ij} = 2\mu \left(\frac{\partial u_i}{\partial x_j} + \frac{\partial u_j}{\partial u_i} \right) \tag{3.3}$$

By expanding the second term of the left side in Equation (3.2)

$$u_j \frac{\partial u_i}{\partial x_j} = \frac{\partial (u_j u_i)}{\partial x} - \frac{\partial u_j}{\partial x_j} = \frac{\partial (u_j u_i)}{\partial x}$$ As mentioned in Eq (3.1)

So the equation 3.2 can be written as

$$\rho \left(\frac{\partial u_i}{\partial t} + \frac{\partial (u_j u_i)}{\partial x_j} \right) = -\frac{\partial p}{\partial x_i} + \frac{\partial}{\partial x_j} (2\mu s_{ij}) \tag{3.4}$$

Where μ= kinematic viscosity and $\mathbf{s}_{ij}$ = strain rate tensor.

Equation (3.1) and (3.4) should be written in time average form as shown below [27].

$$\frac{\partial}{\partial x} \left(U_i + \overline{u_l'} \right) = 0 \tag{3.5}$$

$$\rho \left(\frac{\partial U_i}{\partial t} + \frac{\partial}{\partial x_j} (U_j U_i + \overline{u_j' u_i'}) \right) = -\frac{\partial P}{\partial x_i} + \frac{\partial}{\partial x_j} (2\mu s_{ij}) \tag{3.6}$$

In the above equations, the fluctuating variables hold these properties. $\overline{\boldsymbol{u_l'}} = \mathbf{0}, \overline{\bar{\boldsymbol{u}}_{\boldsymbol{l}}} = \overline{\boldsymbol{u_l}} = \boldsymbol{U_i}$ By eliminating and reorganizing above time average NS, we can rewrite the conservation of mass and momentum equations in the following arrangement [27][30].

$$\frac{\partial U_i}{\partial x_i} = 0 \qquad (3.7)$$

$$\left(\rho \frac{\partial U_i}{\partial t} + \rho \frac{\partial}{\partial x_j}(U_j U_i + \overline{u_j' u_\iota'})\right) = -\frac{1}{\rho}\frac{\partial P}{\partial x_i} + \frac{\partial}{\partial x_j}(2\mu s_{ij}) \qquad (3.8)$$

The new term $\boldsymbol{\rho\, \overline{u_j' u_\iota'}}$ stated in the above equation 3.8 is linked with stress tensor described in previous equations. The term $\boldsymbol{\rho\tau_{ij}}$ is called Reynolds stress tensor and $\boldsymbol{\tau_{ij}}$ is called specific Reynolds stress tensor.

$$\boldsymbol{\tau_{ij}} = -\overline{\boldsymbol{u_j' u_\iota'}}$$

This tensor contains six additional unknown stresses in which three are normal stresses and three are shear stresses. These extra stresses are also known as Reynolds stresses and the set of momentum equations expressed these terms are known as Reynolds-averaged Navier Stokes equation (RANS). In order to solve these six additional unknowns, we have to model some new system equations.

3.1 Turbulence Modelling

Turbulence is usually generated in mean flow due to shear. When the shear is high the turbulence parameters like fluctuating velocity are also high and their behavior is anisotropic in zones near solid walls, the shear is due to wall friction and damping of turbulent velocity variations perpendicular to the boundary. Since all of the flow problems contain solid walls. Hence turbulence configurations are much dependent on geometry. As discussed in the previous part, the tensor $\boldsymbol{\tau_{ij}}$ in RANS equation contains six additional unknowns. These additional unknowns make the system equations open. In order to close these systems of RANS equation, researchers have derived some relations and models of equations. These models are known as turbulence models. Each model has its own characteristics and properties which varies with flow problems. *K*-ω SST is the most useful model for predicting performance in turbo machinery and turbines [23][27]. Hence *K*-ω SST model is selected for present work.

A general way of creating the additional equations is using Boussinesq eddy viscosity

relation [27]. Two new relations are presented to make the RANS system defined [27].

$$k = \frac{1}{2}\overline{v_i v_j}$$

$$\tau_{ij} = \frac{2}{3}k\delta_{ij} - \nu_T\left(\frac{\partial v_i}{\partial x_j} + \frac{\partial v_j}{\partial u_i}\right) \qquad (3.9)$$

Where k = turbulent kinetic energy
ν_T = Kinetic eddy viscosity
δij = Kronecker delta
The values of these depend on the turbulence model used.

The two different dissipation terms are $\varepsilon = C_D k^{\frac{3}{2}}/l = \beta^* \omega k$

Where l = length scale
ε = turbulent dissipation rate
ω = specific turbulent dissipation rate
C_D & β* = closure coefficients

The one turbulence model based on above described eddy viscosity model is *k*-ω shear stress transport model (*k*-ω SST). This model is proposed by Mentor [28]. This model has dual features of *k*-ε and *k*-ω model. *K*-ε turbulence model is unpredictable near-wall zones. However *k*-ω model shows better attributes near wall boundaries. *K*-ω SST model creates a zonal blend, it behaves like *k*-ω model near walls and behaves like *k*-ε model in far field. This two equation model *K*-ω SST shows better behavior under adverse pressure gradient in near-wall zones and wake region. The turbulent kinetic energy and specific dissipation rate equations for this model are expressed below [29].

$$\frac{\partial(\rho k)}{\partial t} + \frac{\partial}{\partial x_i}(\rho k u_i) = \frac{\partial y}{\partial x_j}\left(\Gamma_k \frac{\partial k}{\partial x_j}\right) + G_k - Y_k \qquad (3.10)$$

$$\frac{\partial(\rho \omega)}{\partial t} + \frac{\partial}{\partial x_i}(\rho \omega u_i) = \frac{\partial y}{\partial x_j}\left(\Gamma_\omega \frac{\partial \omega}{\partial x_j}\right) + G_\omega - Y_\omega + D_\omega \qquad (3.11)$$

In eq(3.10) and eq(3.11) Γ_ω & Γ_k = effective diffusivity of ω & k.
G_k= production of turbulent kinetic energy
G_ω= production of ω

Y_ω & Y_k = dissipation of ω & k due to turbulence

D_ω = Cross diffusion term

Effective diffusivity in above Eq (3.10 & 3.11) is computed using following relations [29].

$$\Gamma_\omega = \mu + \frac{\mu_t}{\sigma_\omega}$$

$$\Gamma_k = \mu + \frac{\mu_t}{\sigma_k}$$

Where μ_t= turbulent viscosity

σ_ω & σ_k = Turbulent Prandlt no of ω and k

The turbulent viscosity depends on the magnitude of strain rate and blending function. While the Turbulent Prandtl no depends on blending functions.

Production of turbulent kinetic energy G_k is computed using the procedure defined in k-ω standard model. While the generation of specific dissipation rate is given as $G_\omega = \frac{\alpha}{\nu_T} G_k$ [29].

Dissipation of k and ω is computed using the following expression [29].

$$Y_\omega = \rho\beta\omega^2$$

$$Y_k = \rho\beta^*\omega k$$

β depends on the blending function.

Cross Diffusion term is used to blend the two models k-e standard and k-w standard [29].

$$D_\omega = 2(1 - F_1)\rho\sigma_{\omega,2}\frac{1}{\omega}\frac{\partial k}{\partial x_j}\frac{\partial \omega}{\partial x_j}$$

In the above equation, F_1 is the blending function. The value of blending function varies from 0 to 1. This blending function depends on the cell normal distance from the wall (y). The blending function is calculated such that its value becomes one near the wall, turns on k-w turbulence model. While the value of the blending function is zero in far field, turn on the k-e turbulence model. The model constants $\sigma_{\omega,2}$, $\sigma_{\omega,1}$, $\sigma_{k,2}$, $\sigma_{k,1}$, a_1, $\beta_{i,1}$ and $\beta_{i,2}$ have values prescribed in [29]. While all other constants have the same values as stated for the k-w standard model [30].

The two main factors which separate *K*-ω SST from the *k*-ε and *k*-ω model are cross

diffusion term and blending functions. These characteristics make *K*-ω SST model more reliable and accurate for complex flow problems including transonic shock waves, airfoils and APG (adverse pressure gradient) flows. Moreover, the equations of this model can behave correctly both in far field and near wall regions. The details of *k*-*ε* and *k*-*ω* standard models may be acquired from Wilcox [30].

3.2 Mathematical model of Savonius rotor

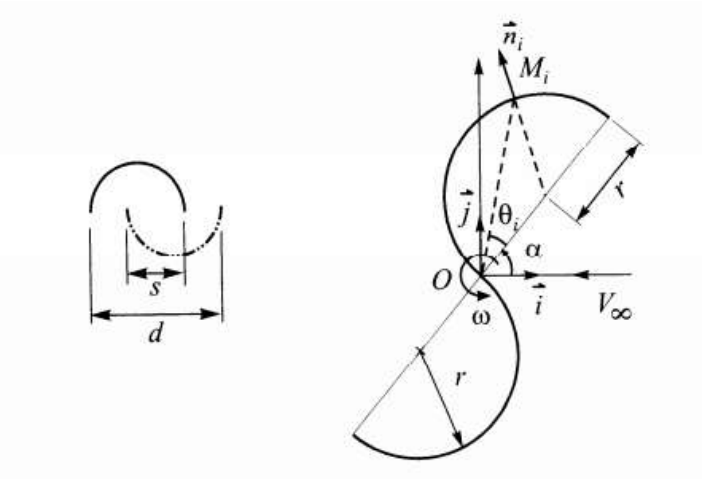

The torque on the rotor is given by.

$$Q = \sum_i \left(\overrightarrow{OM} \times \vec{F_i}\right).\vec{k}$$

It includes two components. i.e. one for returning blade and advancing blade.

$$Q = Q_M + Q_D$$

Total torque in terms of power difference on both blades.

$$Q = 2\,r^2.H \int_0^{\frac{\pi}{2}} (\Delta p_M - \Delta p_D)\ sin\theta d\theta$$

$$P = \ \omega.Q = \frac{\omega}{\pi} \int_0^{\pi} Q\, d\alpha$$

The normalized power coefficient is given by.

$$C_P^* = \frac{P}{{}^1\!/_2\,\rho\, V_\infty^3\,(4rH)}$$

Using the above equations, we can calculate power coefficient as a function of tip speed ratio.

$$C_p^* = [\frac{k\lambda}{2}\frac{1}{2} - \frac{k\lambda^2}{2\pi} + \frac{k-k'}{k}.\frac{\lambda^3}{4}]$$

K is experimentally determined parameter [31].

3.3 Performance parameters and rotor design

In order to compute the efficiency of the turbine appropriately, first we have to discuss design and performance parameters which strongly influence efficiency. The design of savonius HKT is selected from the model used by Hayashi [32]. First, we will discuss the parameters which affect the performance of savonius HKT. After that we will demonstrate the geometric design parameters of savonius rotor used in the present study.

3.3.1 Swept Area:

The swept area is the region of water that surrounds the rotor in its rotation. The shape of the swept area depends on the turbine design. In vertical axis turbines the swept area has a rectangular form and is expressed using this equation:

$$A = H \times D$$

Where

A = Swept area (m^2)

H = Height of rotor (m)

D = Total diameter of rotor (m)

3.3.2 Tip Speed Ratio:

It is the ratio of blade tip velocity (tangential) to the free stream velocity of the water. It is usually written as TSR.

$$\lambda = \frac{R\omega}{V}$$

Where:

R = Radius of a rotor which half of the total diameter (m)

ω = Rotational velocity of rotor (rad/s)

3.3.3 Power, power coefficient and torque coefficient:

The total power available in the water for hydrokinetic turbines can be calculated from the following formula.

$$P_{av} = \frac{1}{2}\,\rho\, A\, V_{\circ}^{3}$$

Where:

ρ = Density of water (kg/m^3)

$V_{\circ}$ = Velocity of the Water (m/s^2)

The power of the rotor as a function of total torque and rotational speed can also be expressed as:

$$P_{rotor} = T\,\omega$$

The power coefficient is the ratio of captured mechanical power by the rotor to the available power in moving water. C_p is known as power coefficient or coefficient of performance

$$C_p = \frac{Power\ captured\ by\ blades}{Available\ power\ in\ moving\ water}$$

$$C_p = \frac{P_r}{P_w} = \frac{P_{Rotor}}{0.5\,\rho\, A\, V_{\circ}^{3}}$$

It can also be written as

$$C_p = \frac{T\,\omega}{0.5\,\rho\, A\, V_{\circ}^{3}}$$

If we multiply and divide the above relation with R i.e. radius of the rotor.

$$C_p = \frac{T\,\omega}{0.5\,\rho\, A\, V_{\circ}^{3}} \times \frac{R}{R}$$

We can also rewrite it as

$$C_p = \frac{T}{0.5\,\rho\, A\, V_{\circ}^{2} R} \times \frac{R\,\omega}{V_o}$$

$$C_p = \frac{T}{0.5\,\rho\, A\, V_{\circ}^{2} R} \times \lambda$$

Now the first non-dimensional term on the right side is known as torque coefficient and denoted by C_m. All other parameters influencing the power coefficient such as AR, blade shape, and overlap ratio have been discussed in chapter 2 with detail.

3.3.4 Geometric representation and parameters of Conventional Savonius rotor

The geometric parameters and model of savonius HKT used in the present study are shown below in Table 3-1 and Figure 3.1.

Table 3-1: Geometric Parameters of rotor

Diameter of rotor [D]	0.330 m
Diameter of blade [d]	0.184 m
No of blades	2
Height of Rotor [H]	0.230 m
Aspect Ratio	0.69
Area of Rotor [m^2]	0.0759
Horizontal Distance between blades (s)	0.038 m
Blade thickness	2mm

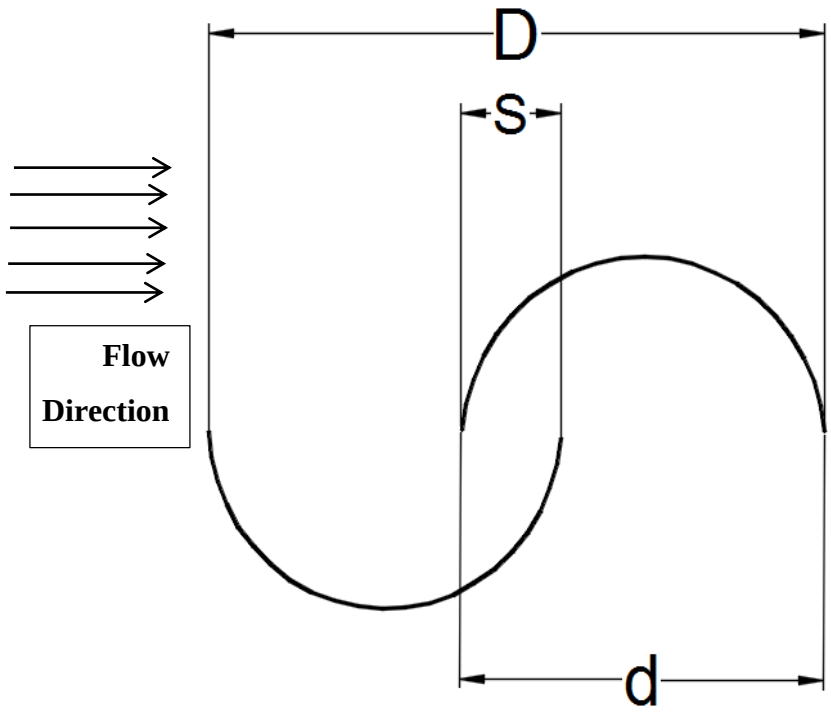

Figure 3.1: Physical 2D Model of Savonius Rotor

The same parameters were used by Hayashi [32] for experimental testing. But Hayashi model contains shaft in the center of blades. However, a recent study of Arifin [33] shows that savonius rotor without shaft performs better than savonius rotor with a shaft in terms of the power coefficient. Hence model of savonius rotor without shaft is selected for the present study. For the purpose of validation study of the CFD model with experimental data, we have selected these parameters of Hayashi [32].

3.4 Computational approach and Boundary settings

CFD analysis is carried out using ANSYS FLUENT [29], which contains incorporates models and schemes for solving turbulent flows. The 2D analysis is chosen for this study as it takes less computational time without considerable depletion of accuracy [34][35]. There are two common methodologies to solve turbo machinery problems numerically.

1. Moving Reference Frame Approach
2. Sliding Mesh Approach

Moving reference frame approach has the capability to solve the system in a steady state manner. This approach is simple and takes less computational time. It contains a rotating reference frame and mesh is stationary. Cell zone creates with respect to moving reference frame.

Sliding Mesh approach is usually used for transient flows and the system is solved in transient manner via time marching. This approach set up a problem in distinct zones which translate or rotate relative to each other. Cell zones rotate relative to each other in little time steps. This approach takes more computational cost but it provides more accurate results than the previous approach as it has the ability to capture unsteady turbulent effects [27]. The sliding mesh approach is mostly used by researchers for the numerical simulation of vertical axis turbines [34][35][36]. Hence sliding mesh technique is adopted in the present study.

A SIMPLE algorithm of pressure velocity coupling is used in this study. It requires less memory and a robust algorithm. The working procedure of the algorithm is shown below in Figure 3.2.

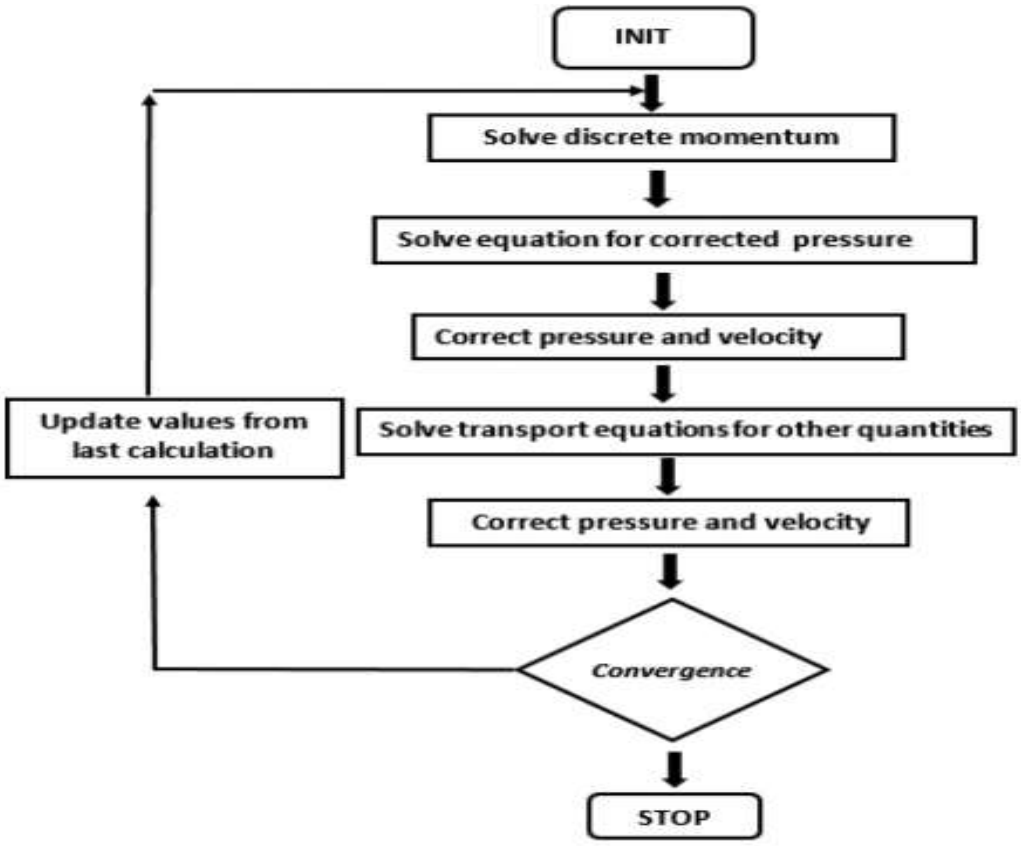

Figure 3.2: Stages of Simple Algorithm [33]

Second order unwinding scheme is used for pressure, momentum, turbulent kinetic energy and dissipation rate equations. As second order schemes provide more reliable and accurate results by reducing numerical errors. A transient FVM solver is selected for the discretization of equations.

3.4.1 Computational Domain:

The domain around the turbine is an important factor for determining the reliable performance parameters. The computational domain around the turbine is divided into two zones. One is a stationary zone and the other is the rotating zone. The large domain takes extra computational time while in small domain boundary conditions influence the turbine performance and leads to inaccurate results. The rotating domain is kept 1.1 times the diameter of the rotor. The velocity inlet is kept 8D from the center of the rotor. The downstream of the rectangular (stationary) domain is created at a distance of 15D from the center of the rotor. The up and bottom domains are kept at a distance of 8D from the center of the rotor. The same computational strategy had been followed by these researchers [36][37]. The physical depiction of the computational

domain is shown below in Figure 3.3.

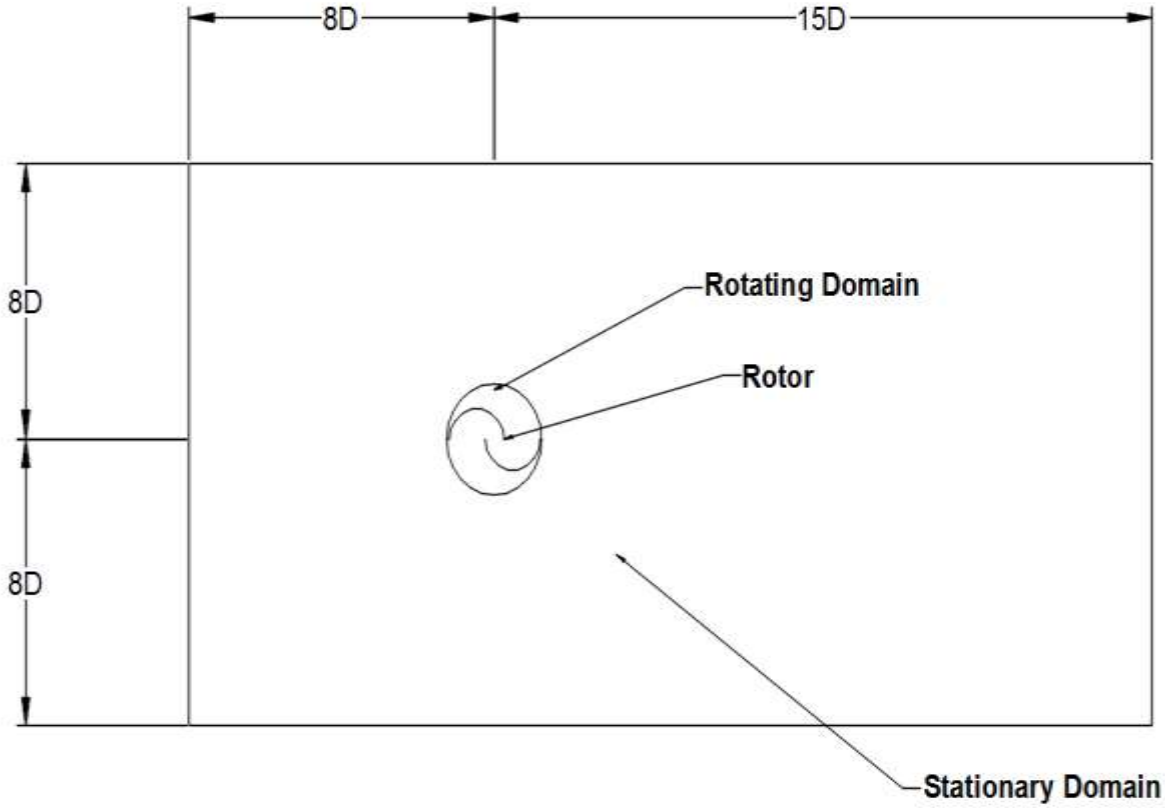

Figure 3.3: Model of computational domain

3.4.2 Boundary conditions:

Boundary conditions play an important role in order to predict the behavior of the flow problem appropriately. Boundary conditions derive the flow problem. In the present study, the boundary conditions are imposed such that the Reynolds number matches with the experimental study. The detailed description of boundary conditions is reported below in table 3-2.

Table 3-2: Boundary conditions

Name	Value	Note
Inlet velocity of Water	0.38 m/s	At inlet wall for initialization
Outlet Pressure	0 Pa	Gage Pressure
Blades	0 rad/sec	No slip walls
Top and bottom sides	-	Symmetry

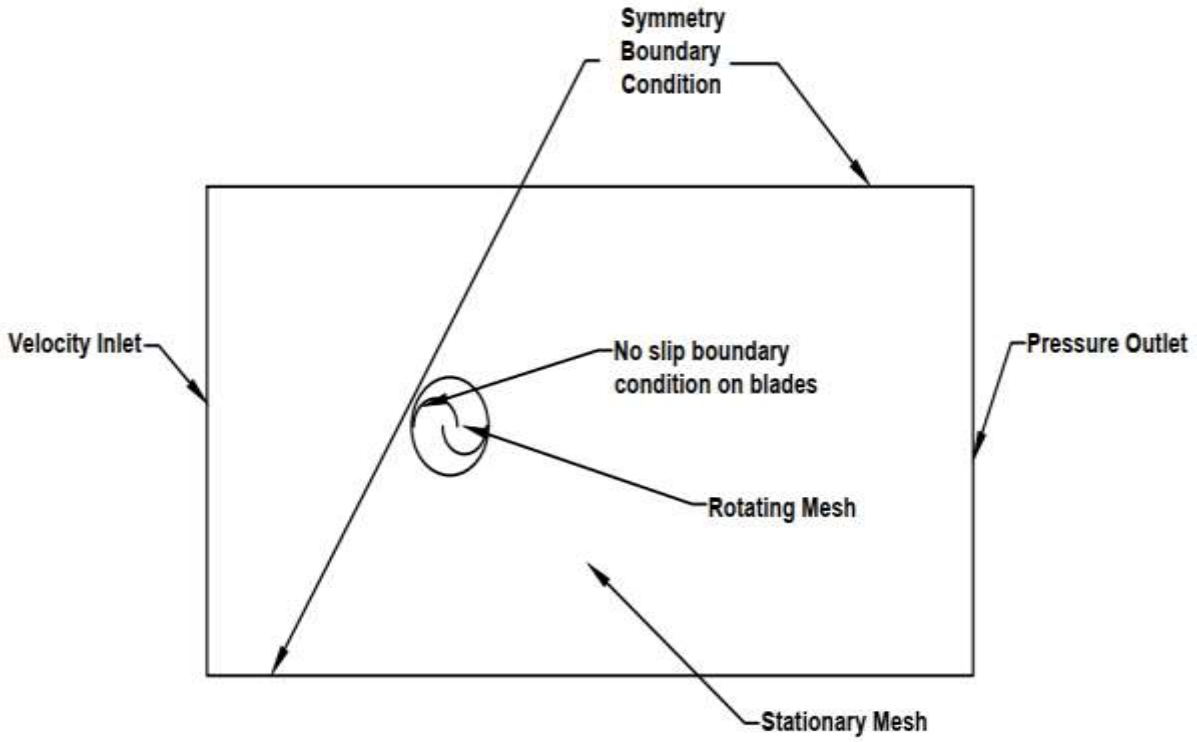

Figure 3.4: Boundary Conditions representation

The physical representation of boundary conditions is shown above in Figure 3.4. The symmetry boundary condition is applied at the top and bottom sides. While blades of the rotor have no slip boundary condition and zero rotational speed relative to rotating cell zone. The details of other boundary conditions are presented above.

3.4.3 Grid generation:

Mesh is an important parameter for the reliable solution of the CFD problem. In the present study, there are two regions of mesh i.e. rotating mesh which is circular domain and stationary mesh the rectangular region. A structured grid provides the most accurate results while it takes more time to set up. Hence an alternate methodology is used. The mesh near the wall region is structured while away from the wall in far field region triangular mesh is imposed. The mesh in the region near the wall of the blade is generated such that the non-dimensional wall distance (y+) should be up to 1. The y+ value selected in a mesh is estimated using the law of the wall. This law is based on empirical results which state that near the wall, velocity inflow changes logarithmically with distance from the wall [30]. The graphical depiction of this law of the wall is shown below in Figure 3.5.

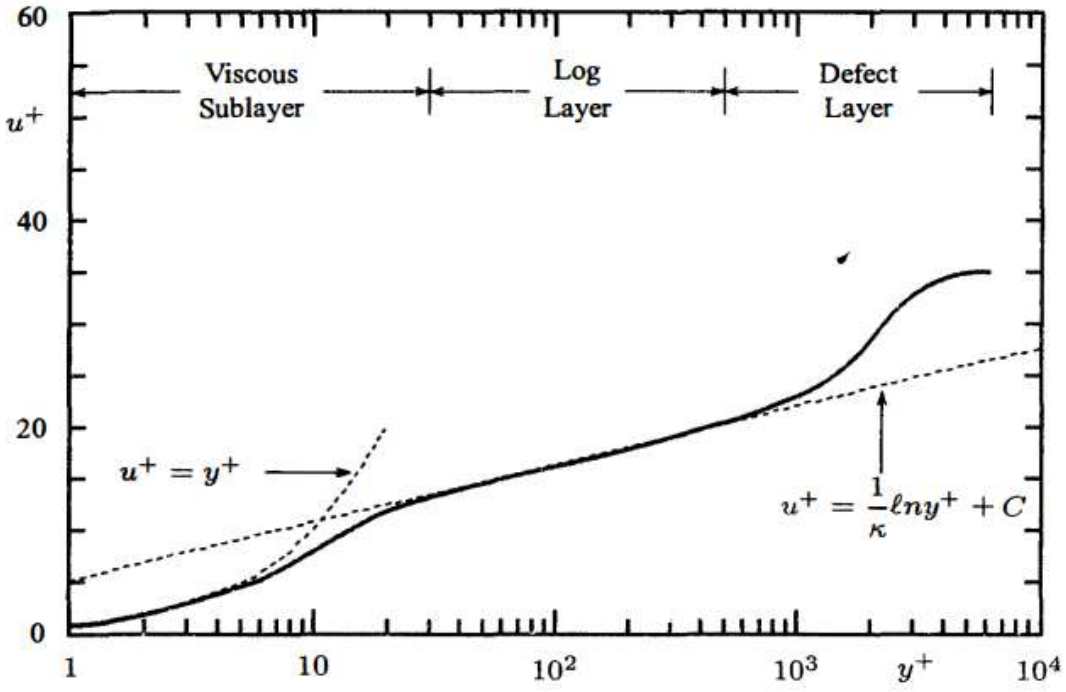

Figure 3.5: Turbulent Boundary layer Velocity Profile

The first cell distance from the wall is estimated using this relation.

$$y \equiv \frac{y^+ \nu}{u_\tau}$$

Where ν = kinematic viscosity

u_τ= friction velocity

And friction velocity is expressed as

$$u_\tau = \sqrt{\frac{\tau_w}{\rho}}$$

Where τ_w = wall shear stress

Wall shear stress is given by

$$\tau_w = C_f \times \frac{1}{2}\rho U^2$$

Where U = free stream velocity

C_f= Skin friction

Skin friction is a function of Reynolds's number

$$\frac{1}{\sqrt{C_f}} = 4\log_{10}(2\,Re_D\sqrt{C_f}) - 1.6$$

This is the whole procedure of calculating the first cell distance from the solid wall.

Hence to obtain y^+ up to one ($y^+ \leq 1$), the 15 layers of structured mesh are applied on the blades. The expansion ratio is 1.1. The first cell distance from the wall computed using the above relations is around 0.03mm. The layers of structured mesh on the wall of the blade is shown below in Figure 3.6. Around the blade, wall mesh is structured (quadrilateral) while away from blades mesh is triangular.

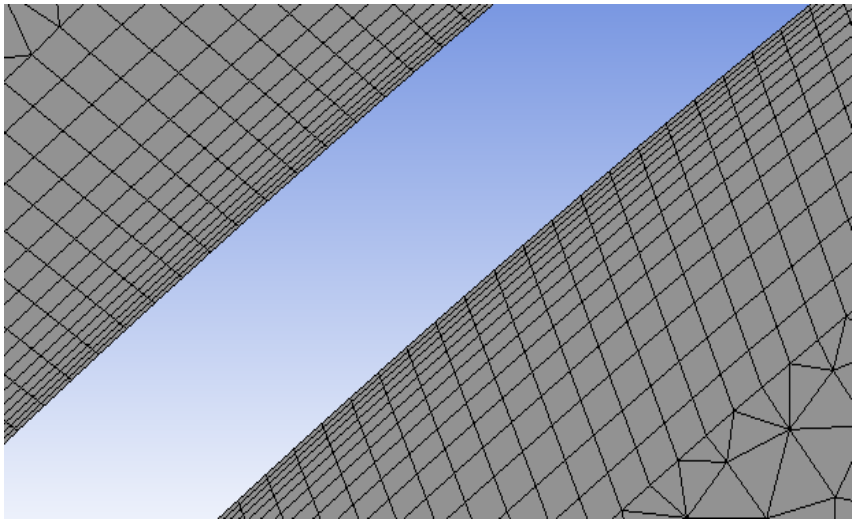

Figure 3.6: Mesh around blades

3.5 Validation Study of CFD Model:

The model of savonius rotor selected for the present study has the same dimensions as used by Hayashi [32]. The Reynolds number of the present study is 1.2×10^5. Water flows with the velocity of 0.38 m/s and boundary conditions used are the same as discussed in previous sections. y+ around the blades is kept up to 1. A SIMPLE algorithm is used with *K*-ω turbulence model.

The solution of the CFD problem should be mesh independent. In order to make a solution mesh independent mesh convergence study has been carried out. Mesh convergence study at tip speed ratio of 0.4 and 0.8 is shown below in the graph.

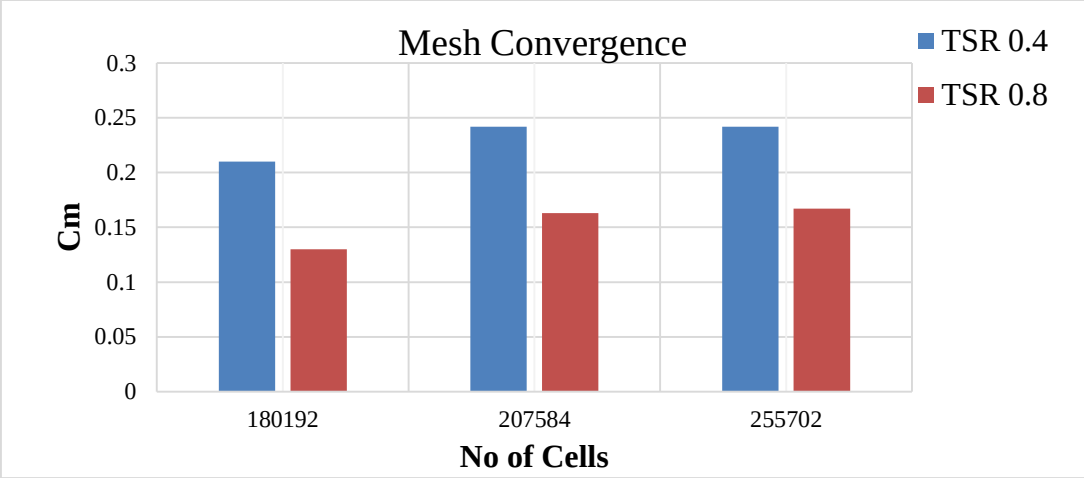

Figure 3.7: Mesh Independence test

Further refinement of the mesh after 0.2 million cells, the coefficient of torque changes about 0.5%. Hence 0.2 million cells are selected for whole simulation work.

Five revolutions have been computed. The first two revolutions have been used to initialize the flow. The average of last two revolutions is used to compute average torque coefficients. The torque coefficient varies too much in the first revolution. After the first revolution, it starts to stabilize. Torque cyclic variation is shown below in Figure 3.8.

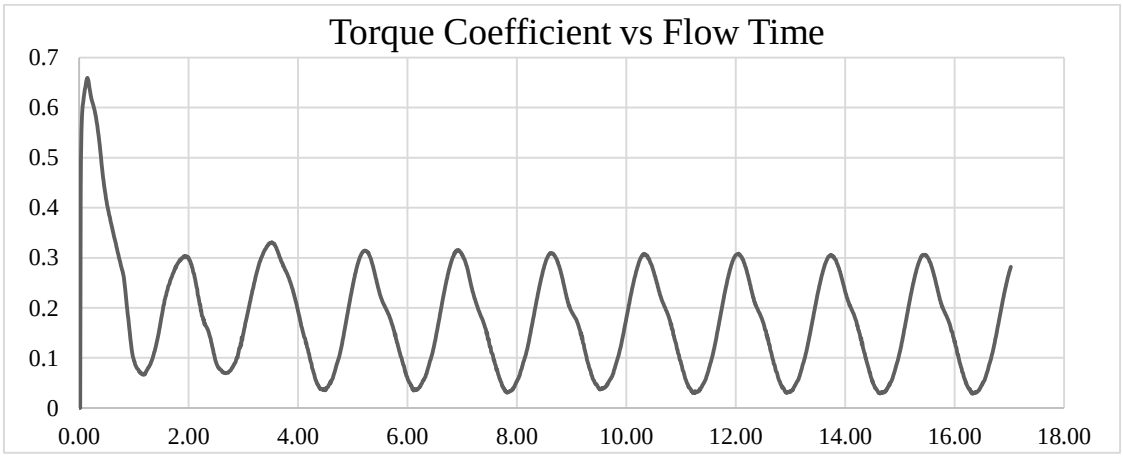

Figure 3.8: Converged results of Torque coefficient

The numerical methods and boundary conditions of the present study have been described in previous sections. A Mesh independence study has been expressed above. *K*-ω SST turbulence model has been selected to tackle turbulence effects. This model is recommended for rotating bodies. Thereafter, the complete numerical analysis has been validated with the existing experimental of Hayashi [32]. Both studies use a conventional savonius rotor for analysis. The comparison between both studies is shown below in Figure 3.9.

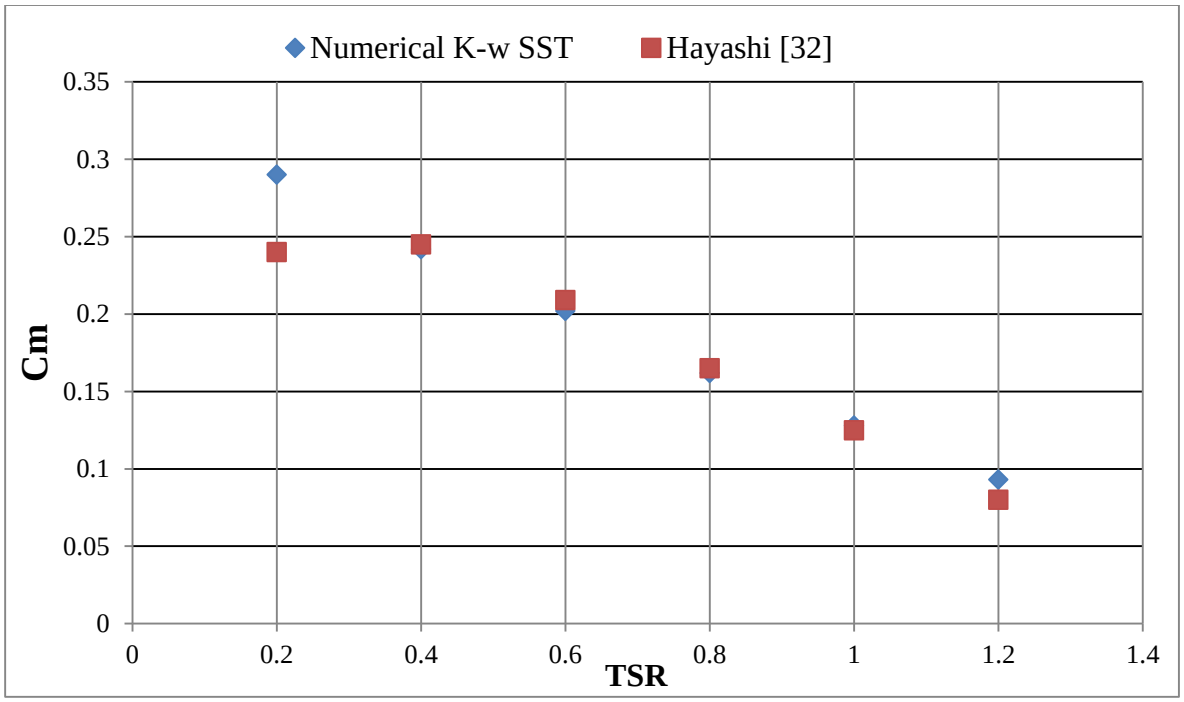

Figure 3.9: Torque Coefficient validation study

The numerical results of Kω-SST show similar behavior with the experimental results of Hayashi. The experimentally measured values agree well with numerical results. At TSR 0.2 and 1.2, the average coefficient of torque obtained from the numerical analysis shows greater values than experimentally measured values. This is due to a lack of shaft in the present study. Savonius rotor without shaft shows better performance than savonius rotor with a shaft as reported in [33].

3.6 Modelling of Proposed Savonius Rotor:

In the current study, the S1048 section profile is chosen for performance improvement. The S1048 profile sketched in the airfoil plotter [38] is shown below in Figure 3.10. The chord of the airfoil is the same as the diameter of the conventional savonius rotor blade. The dimensions of the chord are 184mm.

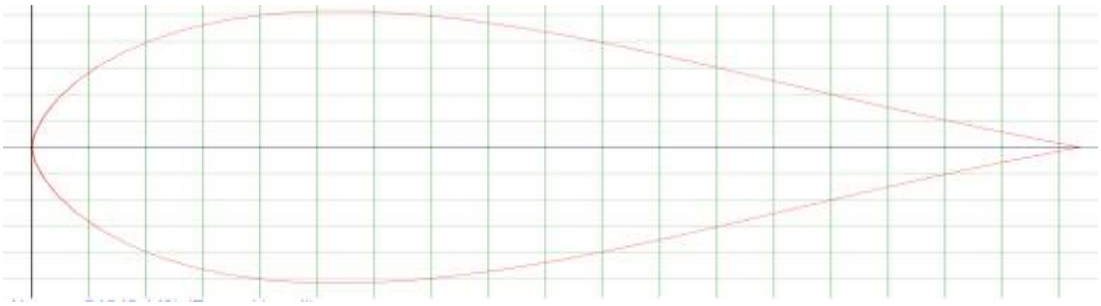

Figure 3.10: S1048 Airfoil

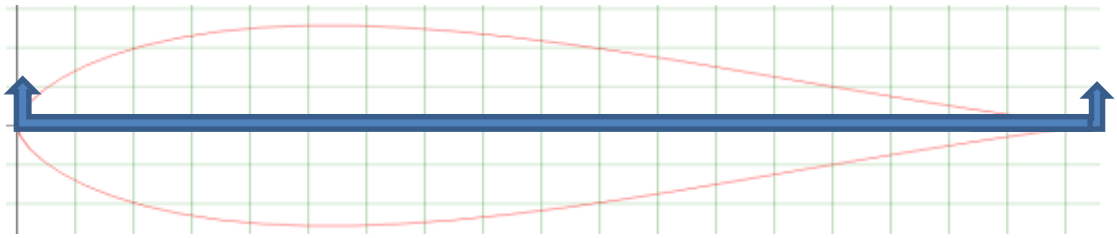

The airfoil shown above is a section cut along the horizontal axis from the origin. The upper part of the airfoil serves as a returning blade while the lower part of the airfoil serves as an advancing blade. All other parameters of the S1048 savonius rotor are same as the conventional savonius rotor as described in previous sections. The 2D model of the S1048 section profile savonius rotor is shown below.

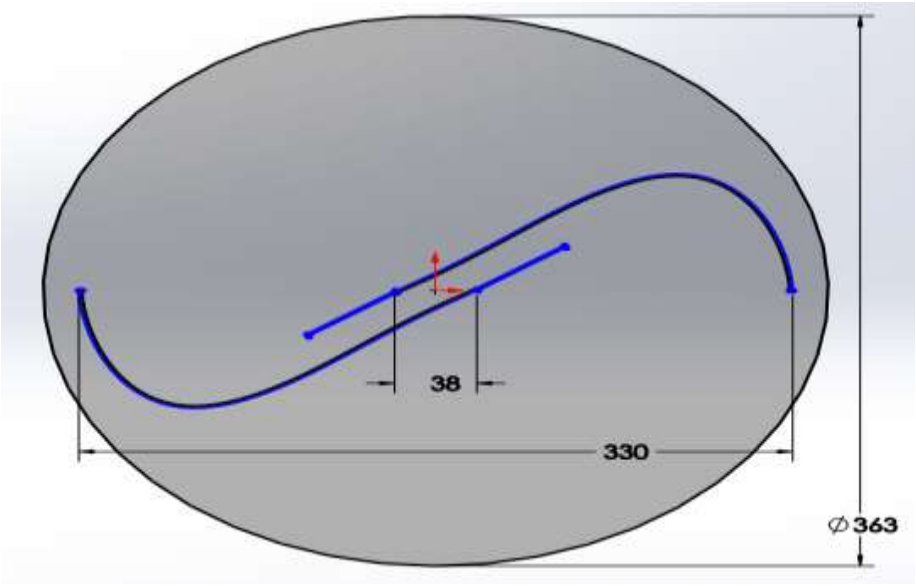

Figure 3.11: S1048 section profile savonius rotor

The S1048 profile savonius rotor is selected for analysis due to the following reasons. Firstly the center of pressure of blades is away from the center of rotation. This larger distance produces larger moment arm, results in greater torque than conventional semicircle savonius rotor. Secondly, the S1048 profile is symmetrical and can easily be manufactured.

3.7 Augmentation Procedure:

As discussed in Chapter 2, the curtain plate design [7] is simple and provides a significant increase in the power coefficient. Altan [7] selected three designs of curtain plates initially. By

experimental testing, they [7] optimized one design. They tested these different curtains in a wind tunnel. The experimental tests were conducted at the average wind speed of 7m/s. In the present study, the dimensions and parameters of curtain design are the same as optimized by Altan [7]. The curtain arrangement is shown below.

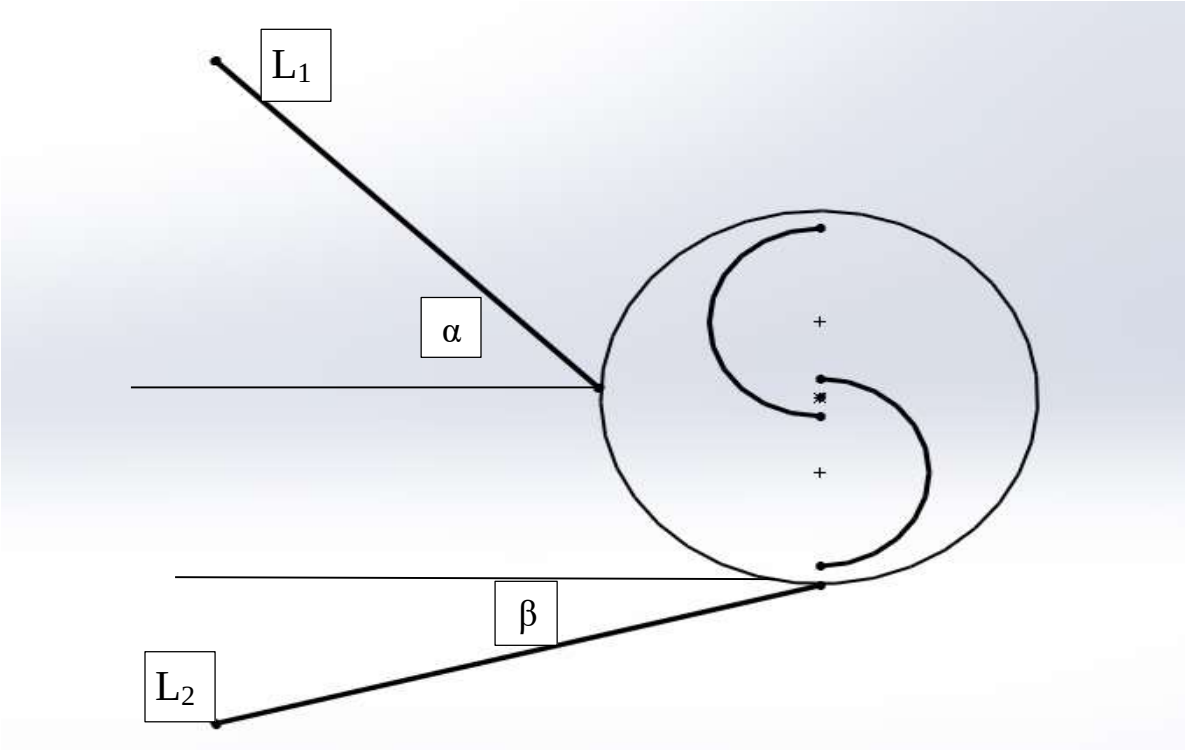

Figure 3.12: Curtain plates design with rotor

Where $L_1 = 45$ cm

$L_2 = 52$ cm

$\alpha = 45$ degree

$\beta = 15$ degree

L_1 and L_2 are the length of curtain plates. α and β are the angles of curtain plates. These lengths and angles are optimized by Altan [7]. The upper curtain plate avoids the generation of negative torque due to the returning blade. Additionally, both the upper and lower plate also serves as a nozzle. This arrangement has the ability to deflect and collect more flow around the rotor.

CHAPTER 4: RESULTS AND DISCUSSION

This chapter will cover the results and extensive discussion obtained after the detailed CFD analysis. This chapter is distributed into two sections the first section will cover the performance and flow physics comparison between S1048 section profile rotor and conventional savonius rotor. The second part will cover the detailed discussion associated with performance enhancement using a curtain plate design.

4.1 S1048 Section rotor and Conventional Savonius rotor:

4.1.1 Performance Characteristics:

In performance characteristics, the torque coefficient and power coefficient are the important parameters. The torque coefficient depends directly on torque. By using a novel S1048 section profile blade, the moment arm increases which results in greater torque. Moreover, the maximum force in conventional savonius rotor acts at the center of the semicircle blade. While in the S1048 section profile rotor, the maximum force shifts toward the tip of the blade. The torque coefficient comparison between the conventional savonius rotor and the S1048 section profile is shown below in Figure 4.1. Torque coefficient for S1048 section rotor is greater than the conventional savonius rotor at all TSR.

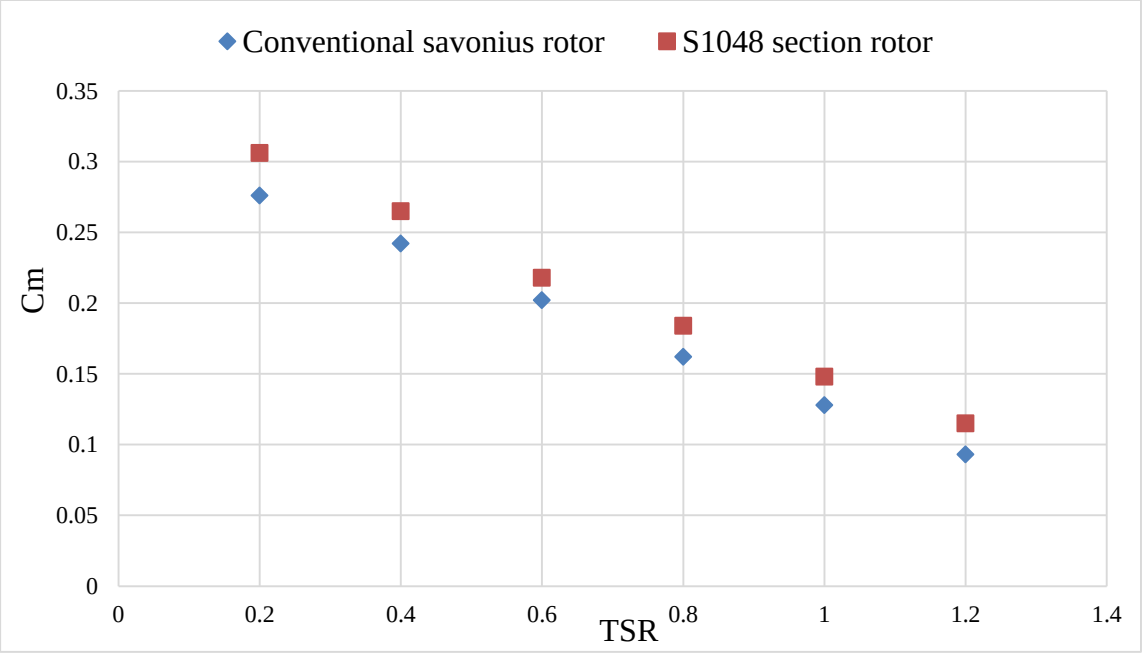

Figure 4.1: Torque Coefficient Comparison between conventional rotor and S1048 section rotor

The power coefficient comparison between the conventional savonius rotor and S1048 section rotor is shown below in Figure 4.2.

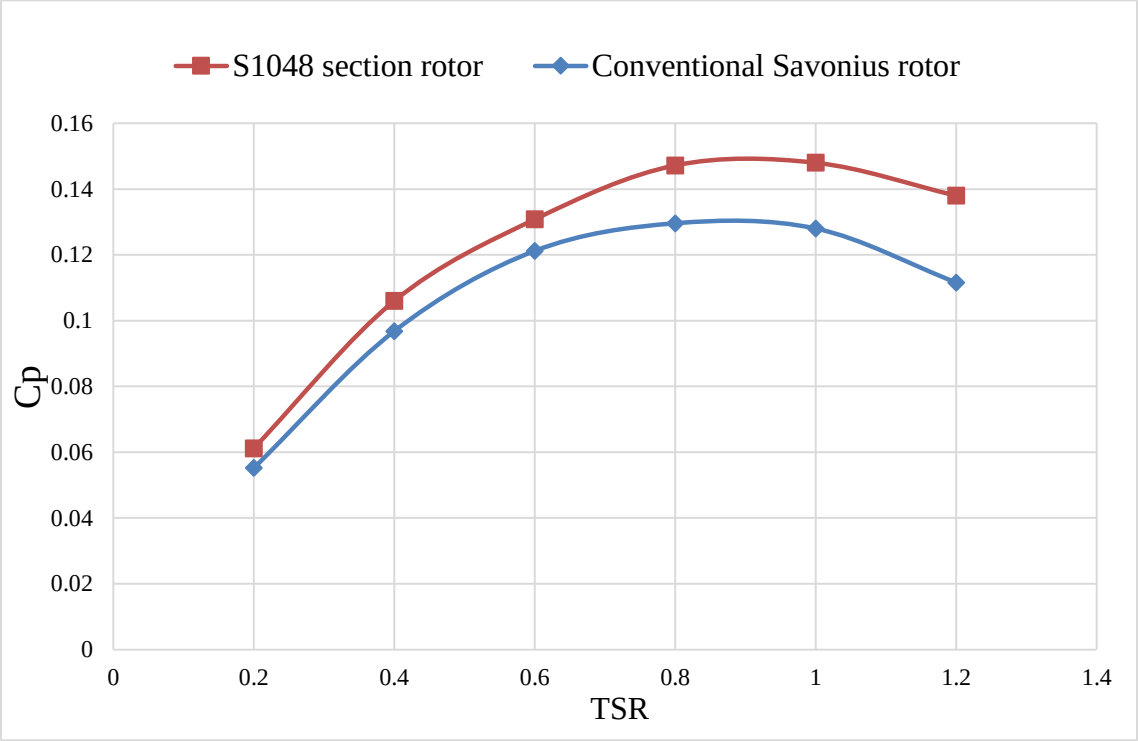

Figure 4.2: Power coefficient comparison between S1048 section rotor and conventional rotor

The power coefficient vs tip speed ratio of both rotors shows a similar pattern. However, the S1048 section rotor has higher values of power coefficient than a conventional rotor at all TSR. The peak power coefficient of the conventional savonius rotor is attained at 0.8 TSR. While in the case of S1048 profile rotor, the peak power coefficient is found at 1 TSR. In addition, the new proposed S1048 section rotor covers a wider range of tip speed ratios. This proposed rotor can operate at wider ranges of tip speed ratio.

The torque coefficient varies with the rotation angle of the rotor. The variation of torque coefficient during one complete cycle at TSR 0.8 is shown below in Figure 4.3. Both configurations show a similar rise and fall in a curve. However, the S1048 section profile has higher peak values than conventional savonius rotor. The peak values of the torque coefficient exist around these angles 15, 200 and 360 degrees. On the other hand, the lowest values are found around these rotor angles 105 and 285 degrees as shown below in Figure 4.3.

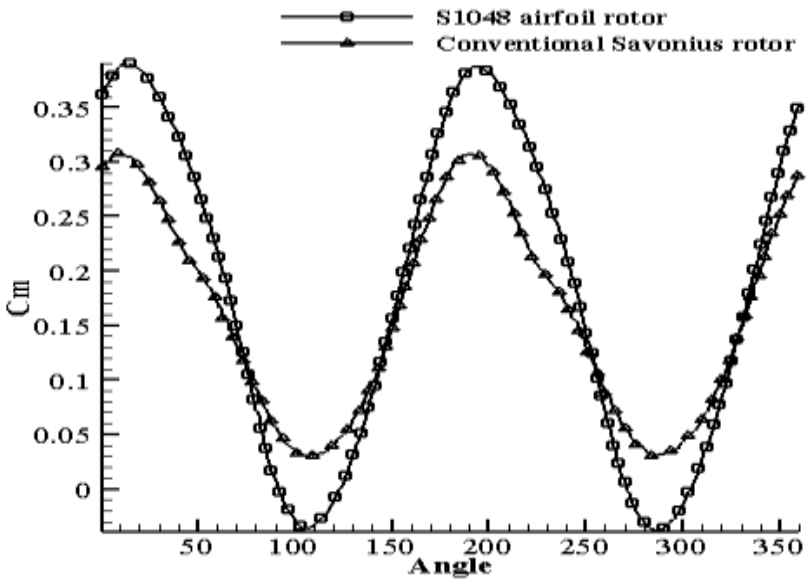

Figure 4.3: Torque coefficient Variation with rotor angle at tsr 0.8

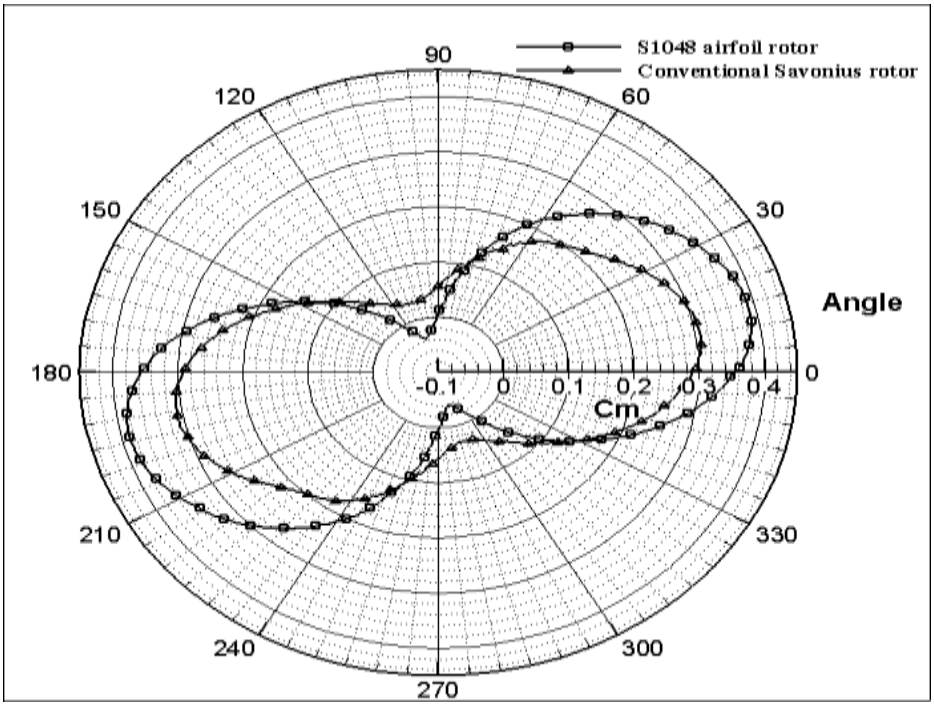

Figure 4.4: Torque coefficient Variation for both rotors at TSR 0.8

Now we will discuss the polar diagram of both types of rotor. The polar diagram shown above represents a variation of torque coefficient during one complete cycle. Torque coefficient of both configurations increases from 0 to 15 degrees and attains peak value of 0.39 and 0.31 for S1048 section rotor and conventional savonius rotor respectively. After that, the torque coefficient starts decreasing. Higher values of C_m are obtained for S1048 section rotor at angular position 0 <

θ < 30 degree and 180 < θ < 210 degree. On the other hand, higher values of Cm is obtained for conventional rotor at angular position 0 < θ < 15 degree and 180 < θ < 195 degree. The lower values of both rotors are obtained at 90 < θ < 120 degree and 270 < θ < 300 degree. A maximum value of Cm=0.39 is achieved for S1048 section rotor at 15 degree rotor angle. These higher values of torque coefficients result in a greater power coefficient.

4.1.2 Pressure Characteristics

To visualize the behavior and performance of the rotors, the pressure is an important parameter. In order to investigate the flow around a newly developed rotor, the analysis of static pressure distribution is carried out for a rotor angle 180 degree. The pressure distribution on blades of both rotors at the rotor angle 180º is shown below in Figure 4.5.

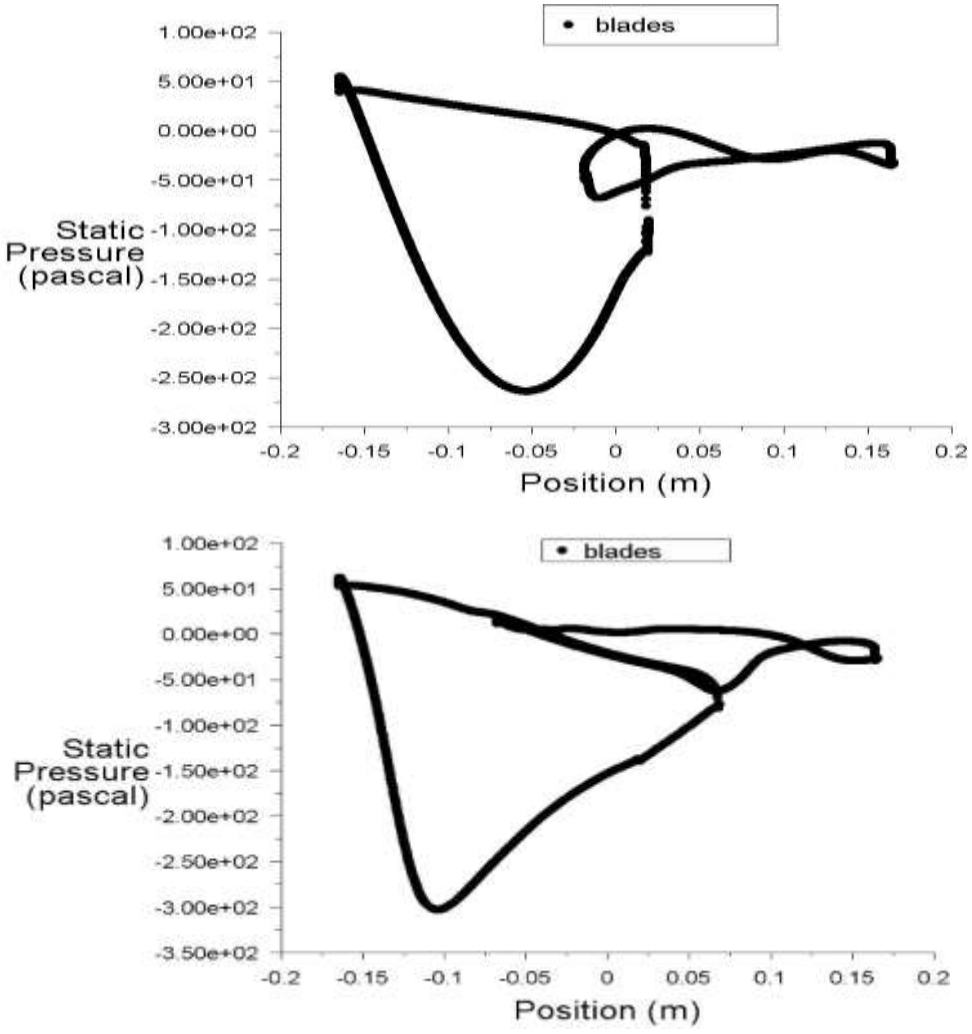

Figure 4.5: Pressure distribution on blade for rotor angle 180º of Conventional savonius rotor and S1048 section rotor

The pressure on the convex side of advancing blades for S1048 rotor and conventional savonius rotor are -305Pa and -264Pa respectively. While near the tip on the concave side of advancing blades, pressure for S1048 rotor and conventional rotor is 63Pa and 55 Pa as shown in Figures 4.5 and 4.6. This large pressure difference for the S1048 rotor provides additional torque. S1048 section rotor is shown on the left side whereas the conventional savonius rotor is shown on the right side.

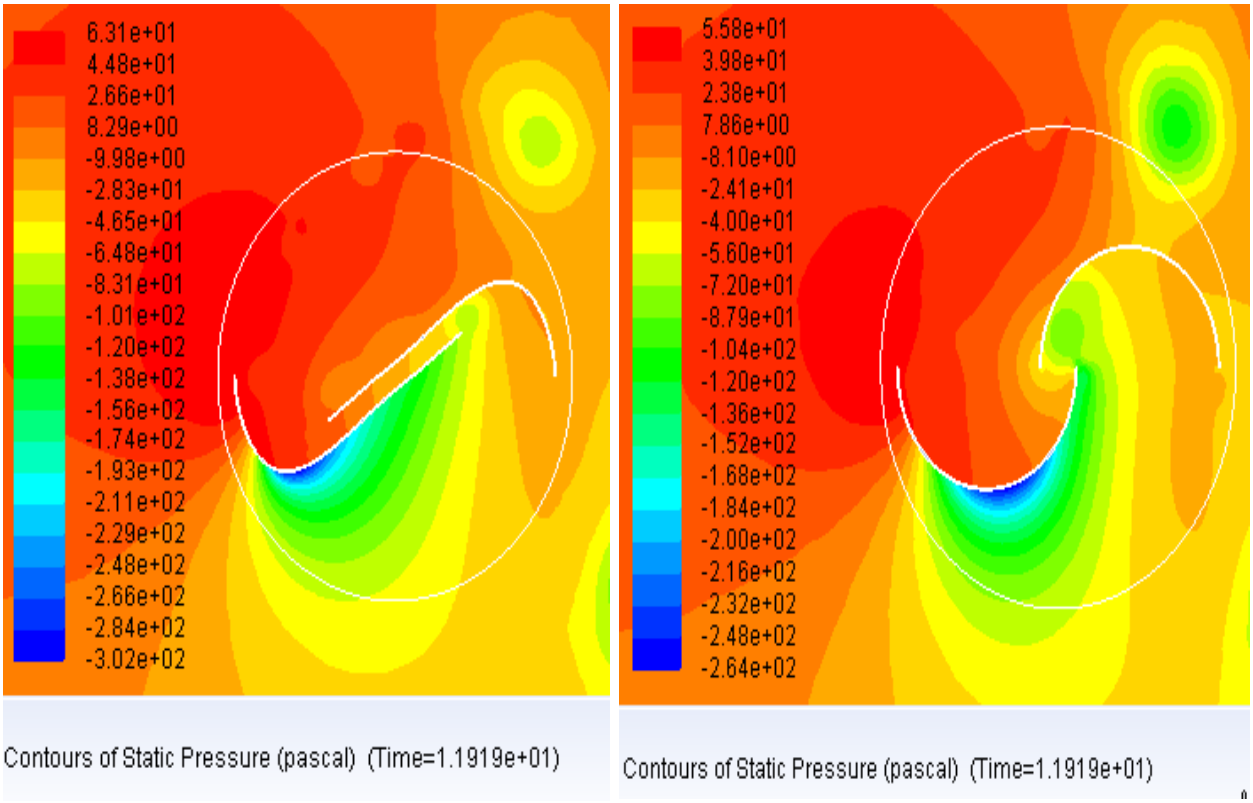

Figure 4.6: Static pressure contours of S1048 section rotor and conventional rotor

Moreover, the convex side of the S1048 section rotor experiences a large pressure difference in comparison with the conventional rotor. This extra pressure difference increases the torque coefficient of the rotor. Furthermore, the convex side of returning blades has a pressure of 82pa and 78pa for S1048 airfoil rotor and conventional rotor respectively. On this side of blade S1048 airfoil rotor depicts higher pressure which in return provides more pressure difference.

Now we will discuss the total pressure around both rotors for rotor angle 30, 90, 150, 210, 270 and 360 degrees. The pressure contours of these rotor angles are shown below in the same order.

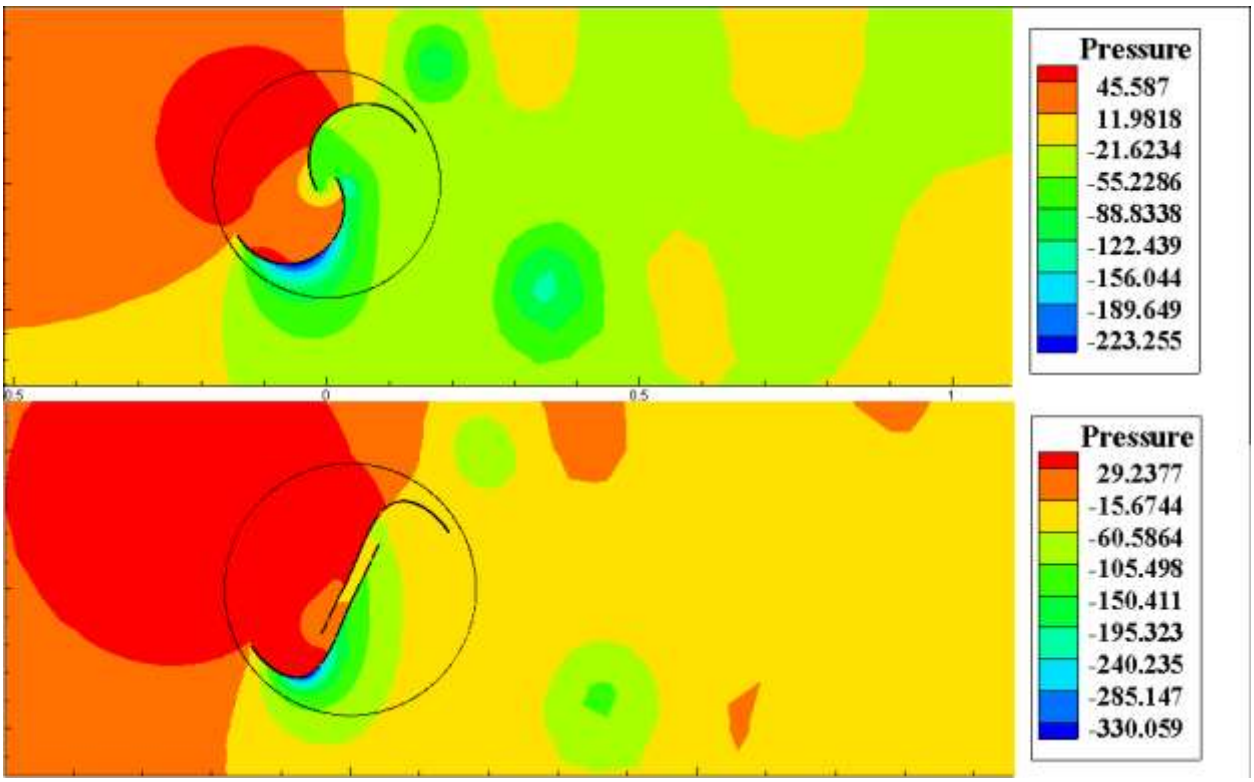
Pressure
45.587
11.9818
-21.6234
-55.2286
-88.8338
-122.439
-156.044
-189.649
-223.255
Pressure
29.2377
-15.6744
-60.5864
-105.498
-150.411
-195.323
-240.235
-285.147
-330.059

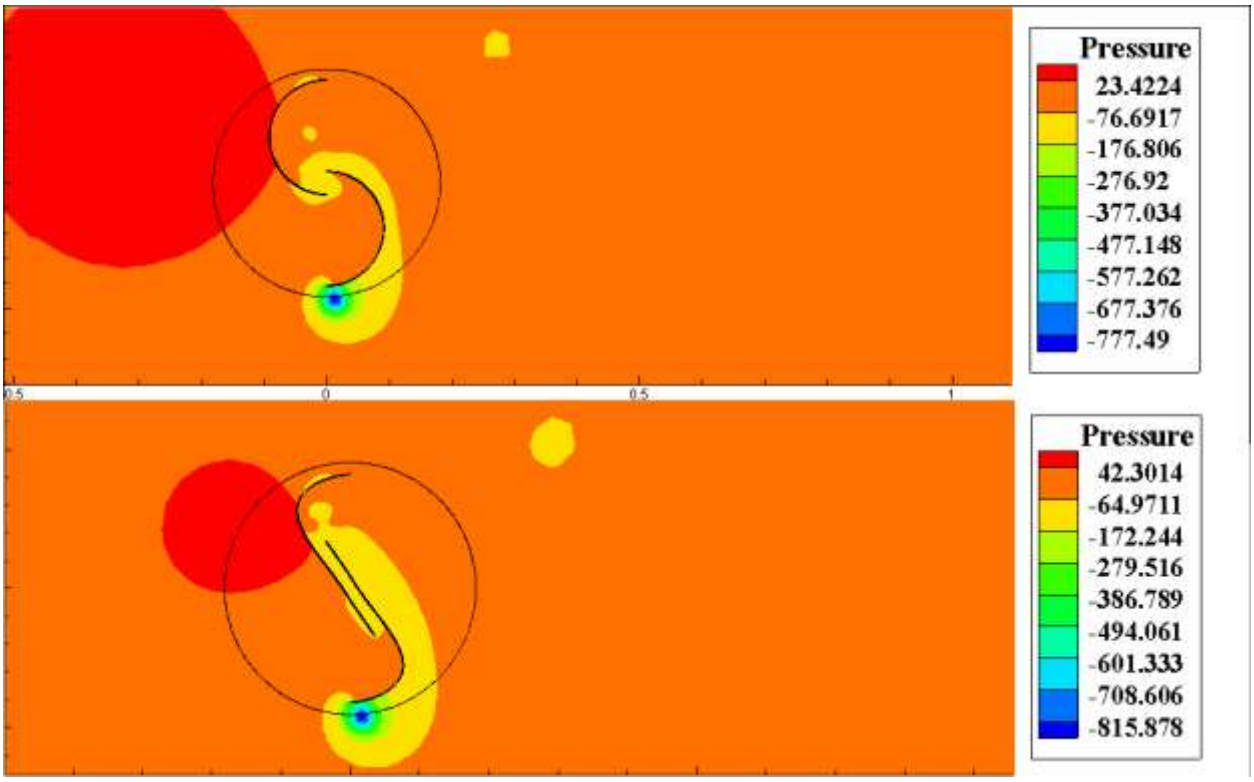
Pressure
23.4224
-76.6917
-176.806
-276.92
-377.034
-477.148
-577.262
-677.376
-777.49
Pressure
42.3014
-64.9711
-172.244
-279.516
-386.789
-494.061
-601.333
-708.606
-815.878

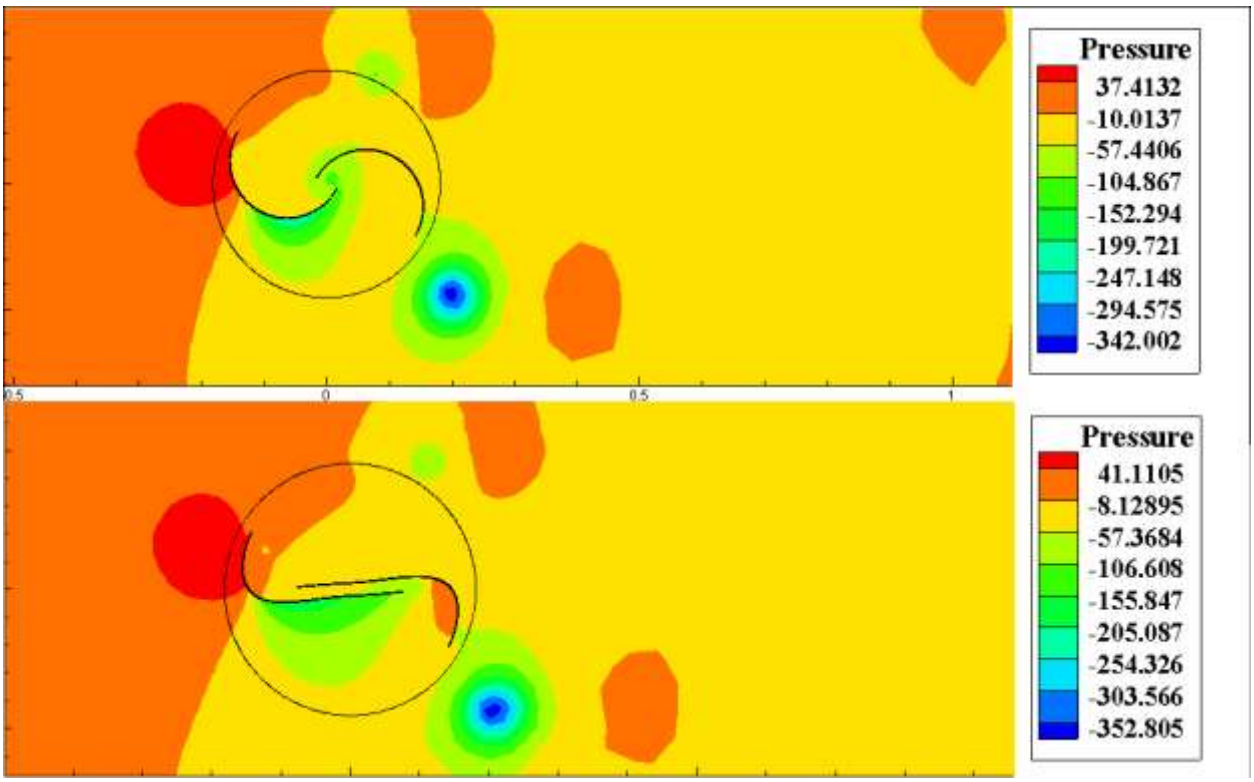
Pressure
37.4132
-10.0137
-57.4406
-104.867
-152.294
-199.721
-247.148
-294.575
-342.002
Pressure
41.1105
-8.12895
-57.3684
-106.608
-155.847
-205.087
-254.326
-303.566
-352.805

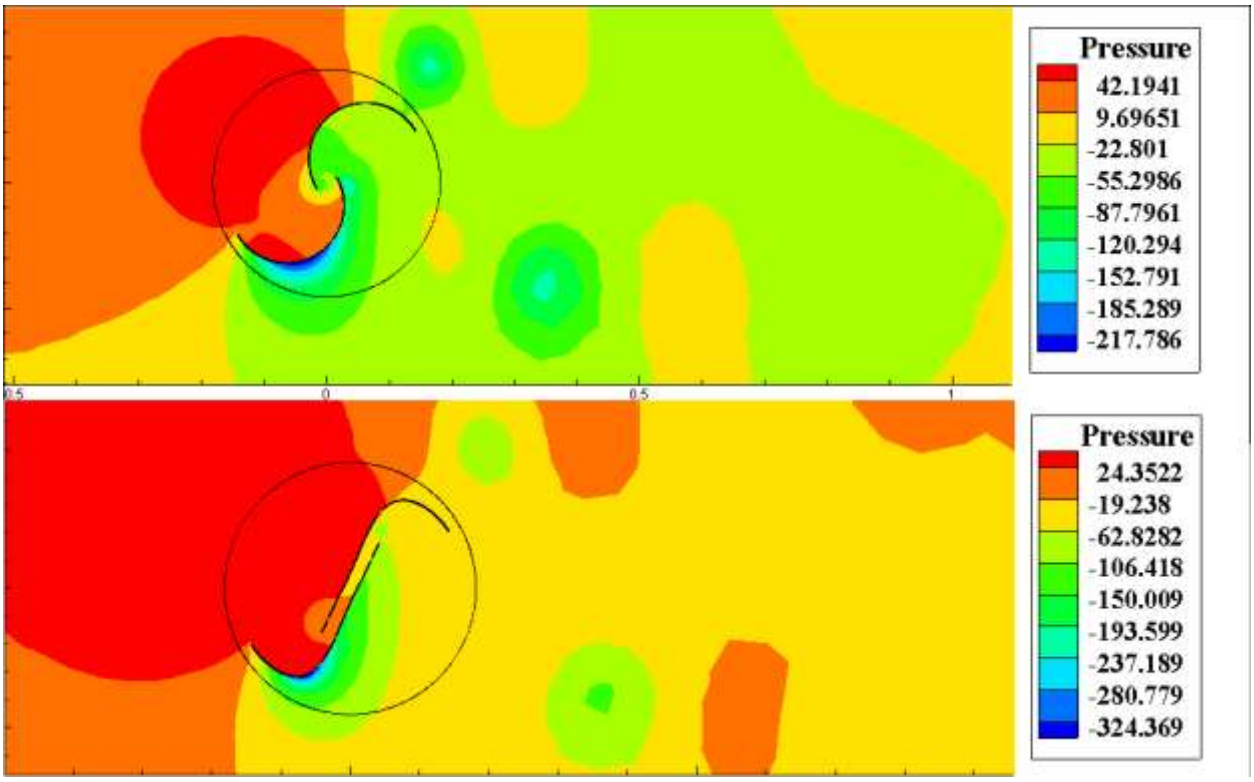
Pressure
42.1941
9.69651
-22.801
-55.2986
-87.7961
-120.294
-152.791
-185.289
-217.786
Pressure
24.3522
-19.238
-62.8282
-106.418
-150.009
-193.599
-237.189
-280.779
-324.369

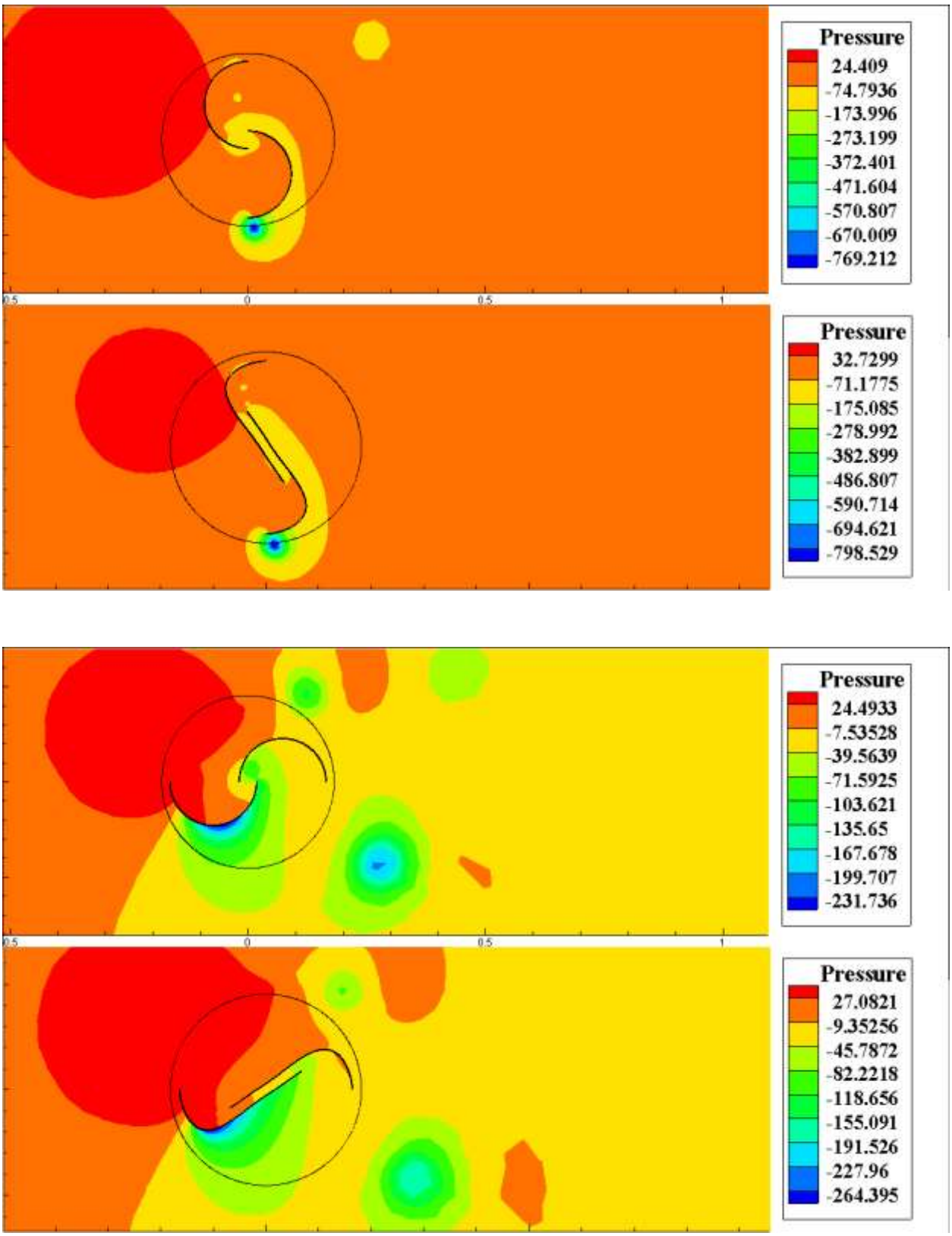

Figure 4.7: Pressure contours of conventional rotor and S1048 section rotor at rotor angle 30, 90, 150, 210, 270 and 360 degree

The conventional savonius rotor is shown on the upper verge of plot while the S1048 section rotor is shown downward. At 30-degree rotor angle, low-pressure region exists at the convex side of the advancing blade in both rotors. However, the value of pressure in the case of S1048 section rotor is lesser than conventional savonius rotor.

Furthermore, near the overlap distance, conventional savonius rotor experiences a low-pressure region while S1048 section rotor has a higher pressure regime at this location. At rotor angle 90 degree, low-pressure region exists near the tip of advancing blade for both rotors. But the intensity of pressure in the case of S1048 section rotor is smaller than conventional rotor. This less pressure provides a larger pressure difference for S1048 section rotor. At 150 degree rotor angle, the maximum value of pressure is obtained at the tip of returning blade in both rotors. But the S1048 section rotor covers an additional high pressure zone in this area. All other flow pattern seems similar for both rotors. For the rotor angle 210 degrees, higher pressure values are obtained at the left side of both rotors.

However low-pressure region attains at the convex side of returning blade and the S1048 section profile has lesser pressure values. At the rotor angle 270 degrees, the flow patterns are similar to rotation angle 90 degrees. Higher values of pressure are found near the convex side of returning blades. Moreover, this value of pressure is greater for S1048 section rotor. At the rotor angle 360 degree, the low-pressure region is found near the convex side of the advancing blade.

Moreover, near the overlap distance, the pressure is greater in the case of S1048 section rotor. From the above contour plots, it has been seen that at rotor angle 30 degree the pressure on the advancing blade is comparatively higher than the pressure on returning blade. As the rotation angle increases the pressure on advancing blade increases while the pressure on returning blade decreases. At a certain angle, the total pressure difference is higher hence at that location rotor attains maximum torque.

4.1.3 Velocity Characteristics:

Velocity contours around the blades are an important parameter for predicting flow features of the rotor. The comparison of the velocity field between conventional savonius rotor and S1048 section rotor is analyzed. The velocity contours at the rotor angle 30 degree is shown below in

Figure 4.8.

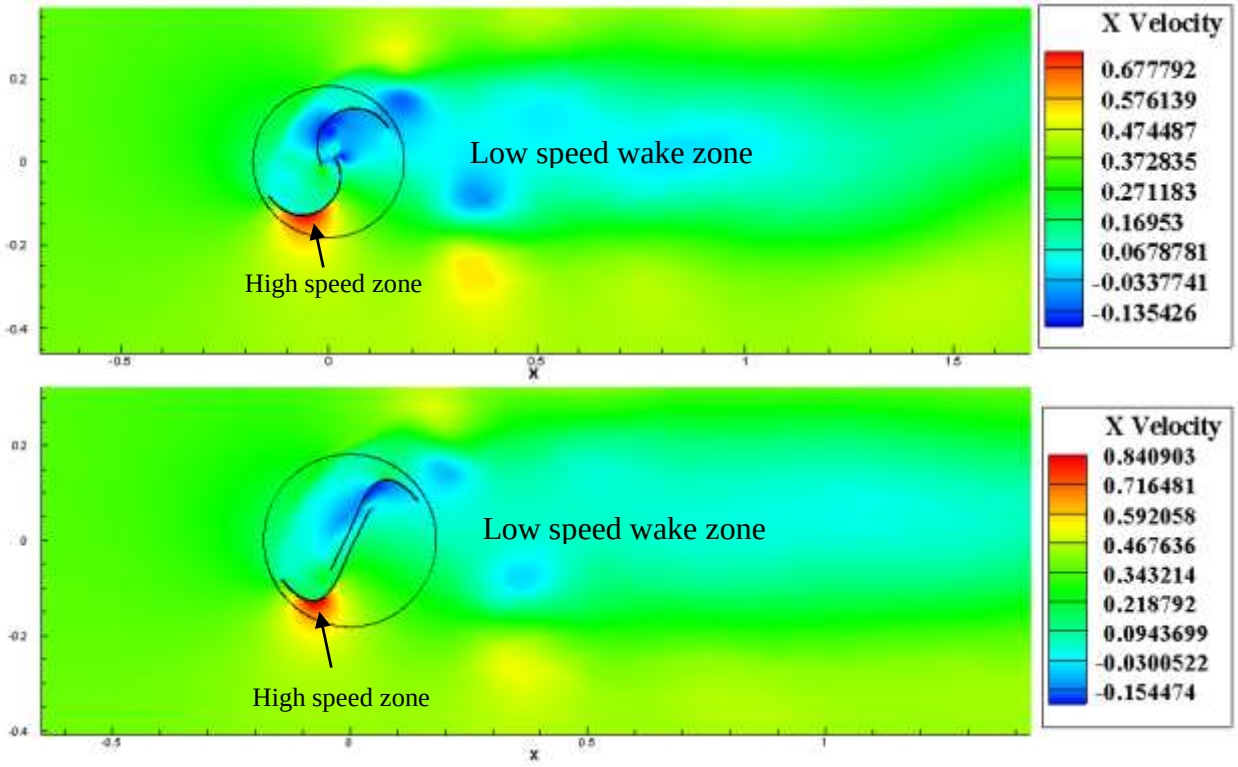

Figure 4.8: Velocity contours of S1048 section rotor and conventional rotor at rotor angle 30 degree

At the rotor angle 30 degree, the velocity at the left hand side is same as the inlet velocity specified in boundary condition. The maximum velocity zone has been found near the tip of the advancing blade. The Magnitude of tip velocity is higher for S1048 section rotor. Low velocity zone or wake zone exists behind the rotor in downstream. The length of the wake region is larger in the case of S1048 section rotor. The velocity contour for rotor angle 90 and 210 are discussed below in Figure 4.9.

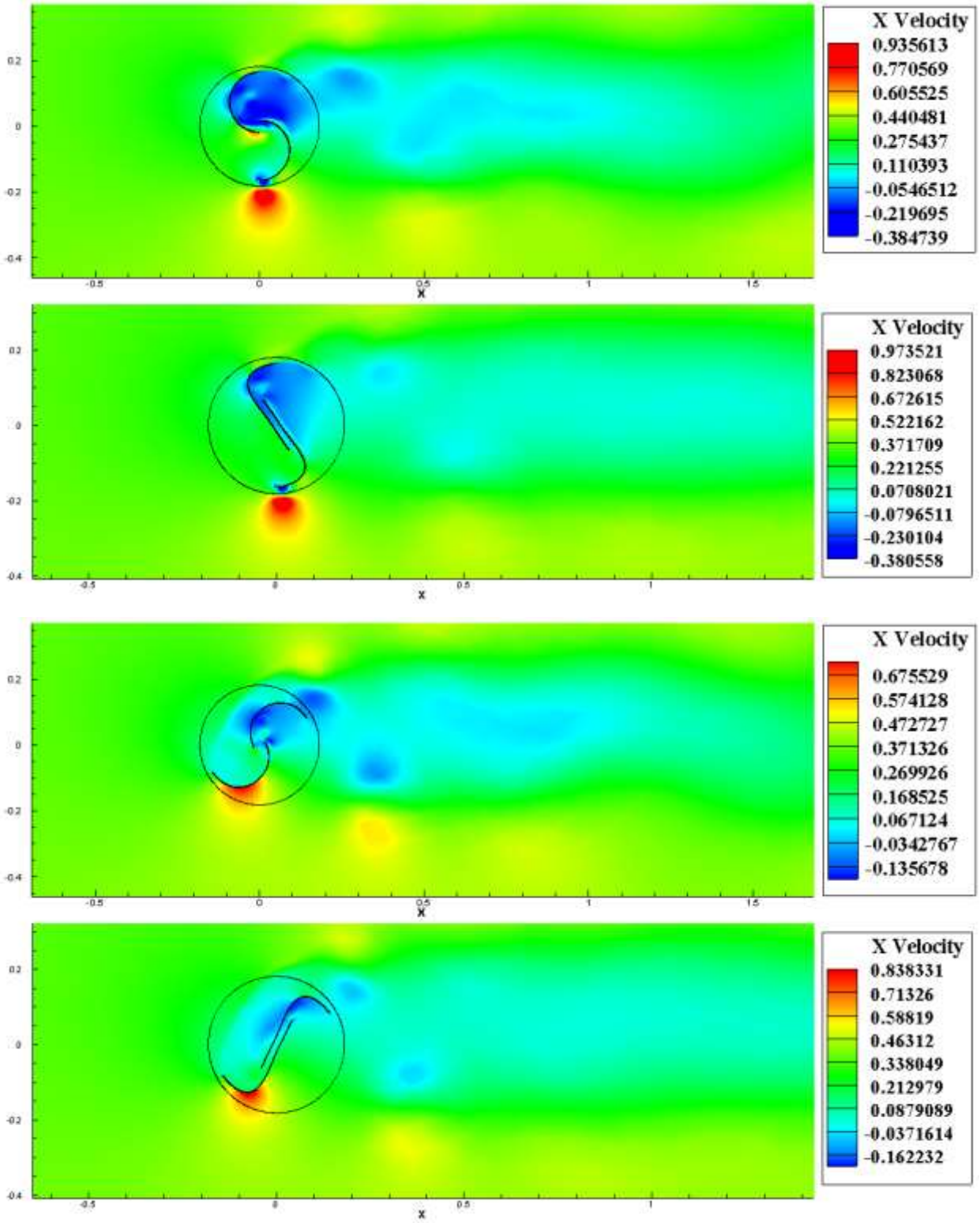

Figure 4.9: Velocity contours of conventional rotor and S1048 section rotor at rotor angle 90 & 210

As shown above, the high-speed zone is found at the tip of advancing blade. The intensity of this zone is higher for S1048 section rotor. The stagnation point is obtained on the convex side of the returning blade. At rotor angle 210 degree, velocity field is same as described for 30 degree. Furthermore, for the rotor angle 360 degree, the contour plots are shown below.

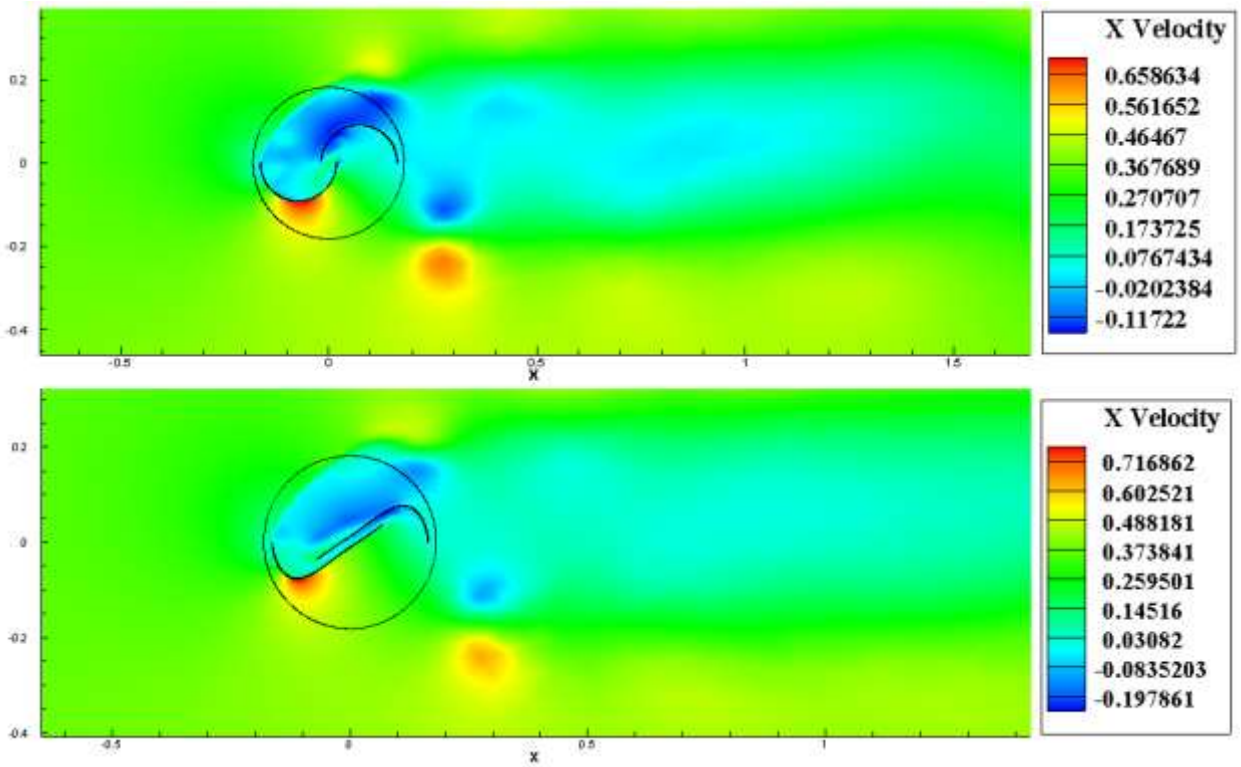

Figure 4.10: Velocity contours of conventional rotor and S1048 section rotor at rotor angle 360 degree

At 360 degree the magnitude of velocity at tip of the blade is higher for S1048 section rotor. The general difference between the velocity field of S1048 section rotor and conventional rotor is described as.

1. The S1048 section rotor has a higher magnitude of tip vortices. Due to this reason pressure reduction is high on the convex side of the blade.
2. The S1048 section rotor has a wider low speed wake zone which leads to extra pressure drop in the downstream region due to adverse pressure gradient.
3. The stagnation point in S1048 section rotor has shifted towards the tip of the blade which leads to higher pressure in this region.

4.1.4 Vorticity Characteristics:

As elaborated previously, the newly proposed blade profile has a higher power coefficient which results in extra pressure drop and higher velocity distribution on blades. Vorticity is basically the curl of velocity vector.

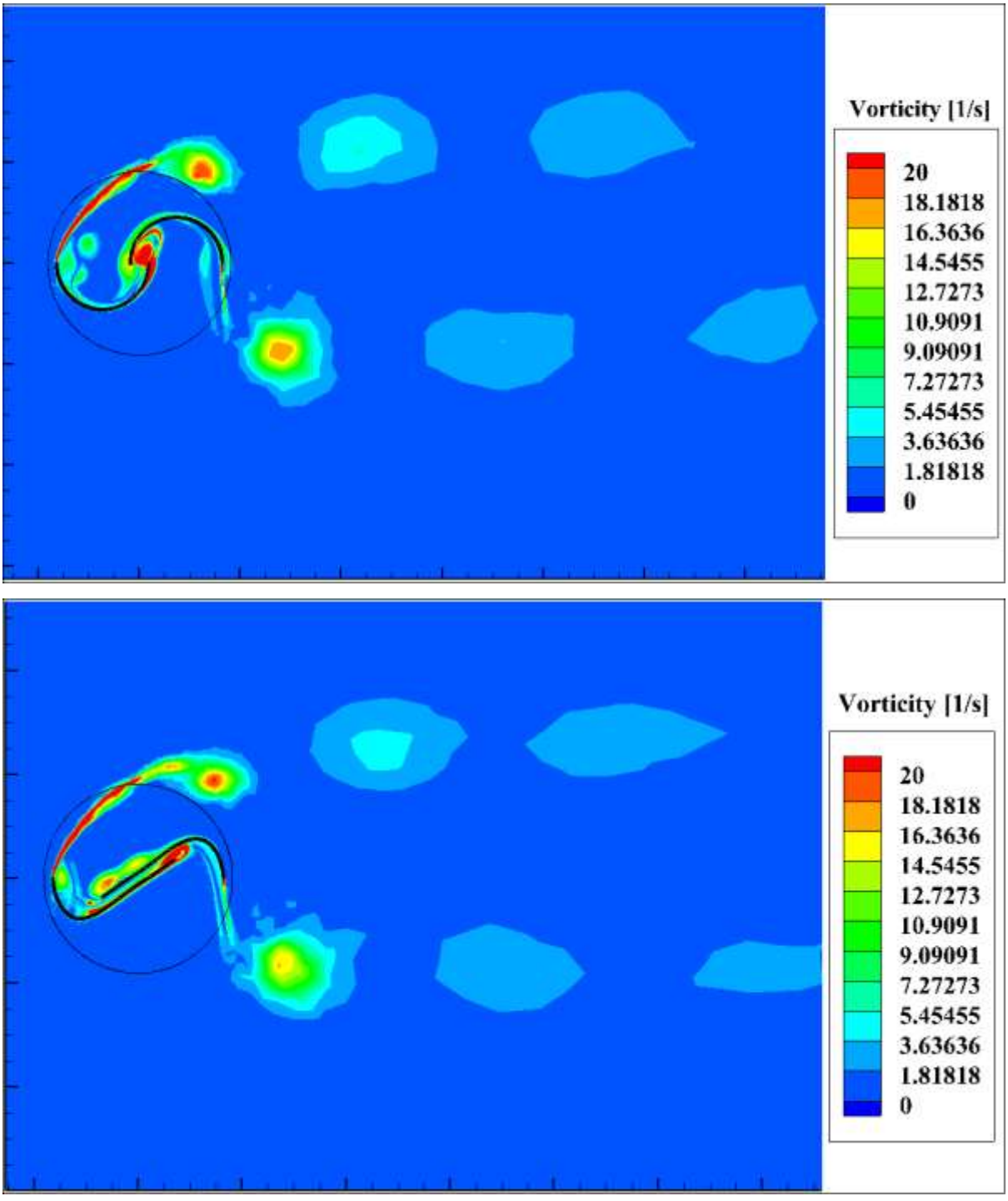

Figure 4.11: Vorticity contours of conventional rotor and S1048 section rotor

The vorticity contours at tip speed ratio of 0.8 for rotor angle 360 are shown above. The range of vorticity is from 5.512804e-05 to 4792.068 (1/s). In order to visualize the contours properly, the maximum value of 20 (1/s) is used. Both rotors show almost similar flow pattern at upstream and downstream of the rotor. Vortices dissipate rapidly by increasing downstream distance. However, for conventional savonius rotor the greater intensity of vortices is found near the overlap distance between the blades. Conversely, for S1048 section rotor, the greater intensity of vortices is found on the concave side of the returning blade. Therefore pressure on this side of proposed blade decreases. Hence the proposed blade profile has a greater power coefficient.

4.2 Rotors with Augmentation device:

In the previous chapter, we have discussed the configuration of curtain plate augmenter. In this section will discuss the flow field characteristics of both rotors using curtain plate design. Curtain plate design increases the flow velocity and also acts as deflector which diminishes the negative torque generated by returning blade.

4.2.1 Performance Characteristics:

The curtain plates design increases the torque coefficient of the rotor which as a result intensifies the coefficient of performance. The comparison of the power coefficient between rotors without augmentation and rotors with a curtain plate design is shown below in Figure 4.12.

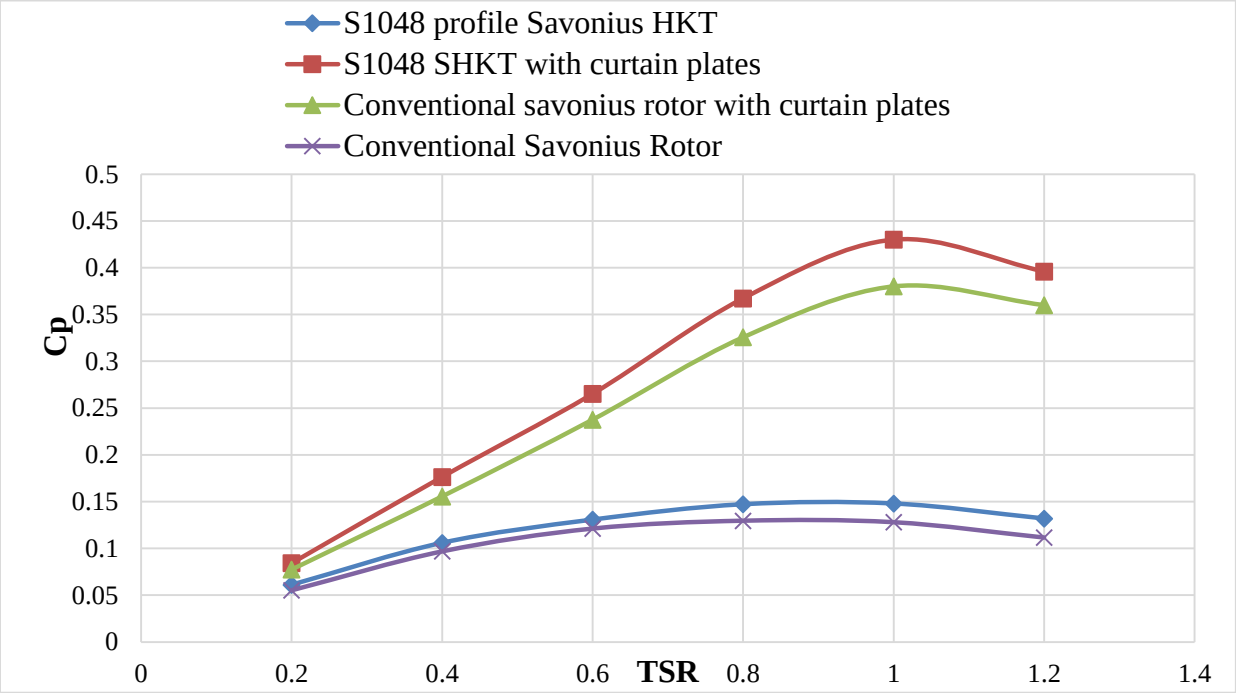

Figure 4.12: Power coefficient comparison between un-curtain rotors and rotors with curtain plates

As shown above, the power coefficient of the conventional savonius rotor with curtain plates is enhanced significantly when augmentation is used. The trend of the graph shows a resemblance to the performance plot evaluated by Altan [7]. By increasing the tip speed ratio the power coefficient increases. For the conventional savonius rotor with curtain plates, the maximum power coefficient is achieved at a tip speed ratio of 1 and has a value of 0.38. Conversely, the S1048 section rotor has a maximum power coefficient of 0.43 at a tip speed ratio of 1. Moreover, the power coefficient increases with increasing tip speed ratio for both rotors with curtain plates. After a tip speed ratio of 1, the power coefficient starts decreasing. The S1048 section rotor with curtains has 13% higher power coefficient than a conventional savonius rotor with curtains. The polar diagram of conventional savonius rotor and S1048 section rotor with curtain plates are shown below in Figure 4.13.

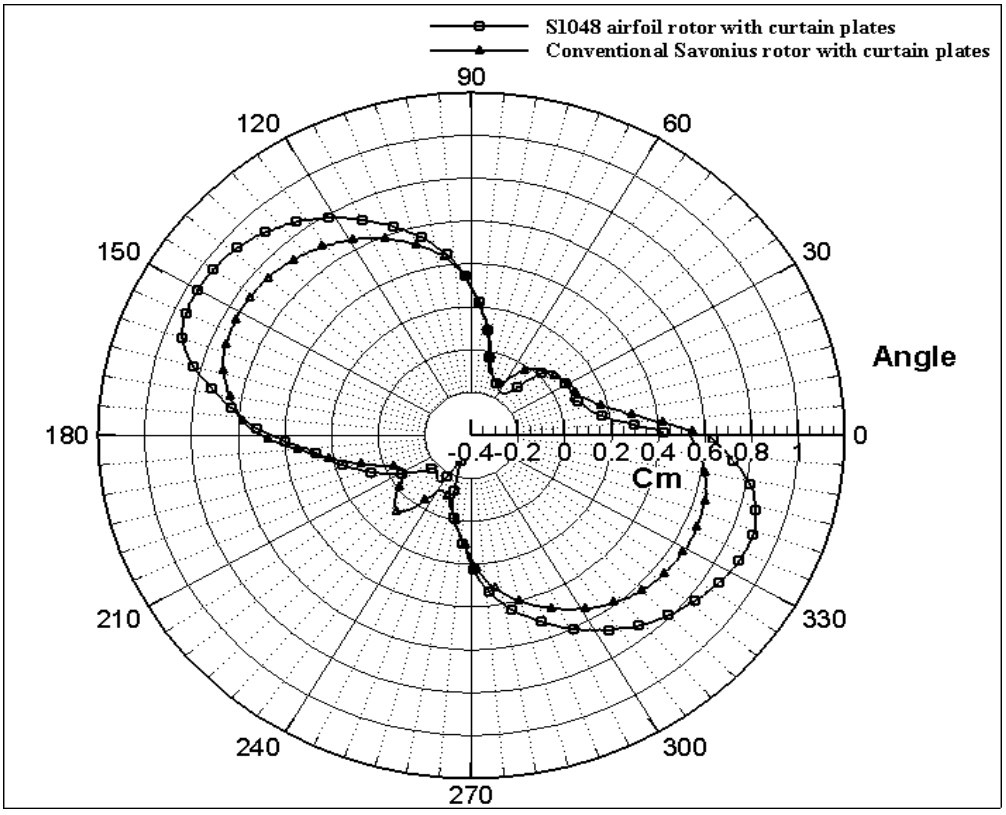

Figure 4.13: Torque coefficient variation rotor angle for conventional and S108 section rotor with curtain arrangement

The polar diagram shown above represents the variation of torque coefficient over one complete cycle. Torque coefficient of both configurations with curtain plates increases from 90 to

120 degree and attains peak value of 0.9 and 0.75 for S1048 section rotor and conventional savonius rotor respectively. After that, the torque coefficient starts decreasing. Higher values of Cm is obtained for S1048 section rotor and conventional rotor at angular position $90 < \theta < 150$ degree and $290 < \theta < 360$ degree. A maximum value of Cm=0.9 is achieved for S1048 section rotor at a 150 degree rotor angle. These higher values of torque coefficients result in greater power coefficient of 0.43 which is 13% higher than conventional rotor with curtain plates.

4.2.2 Pressure Characteristics:

The pressure variations through the un-curtain rotor and rotor with curtain are shown below in Figure 4.14.

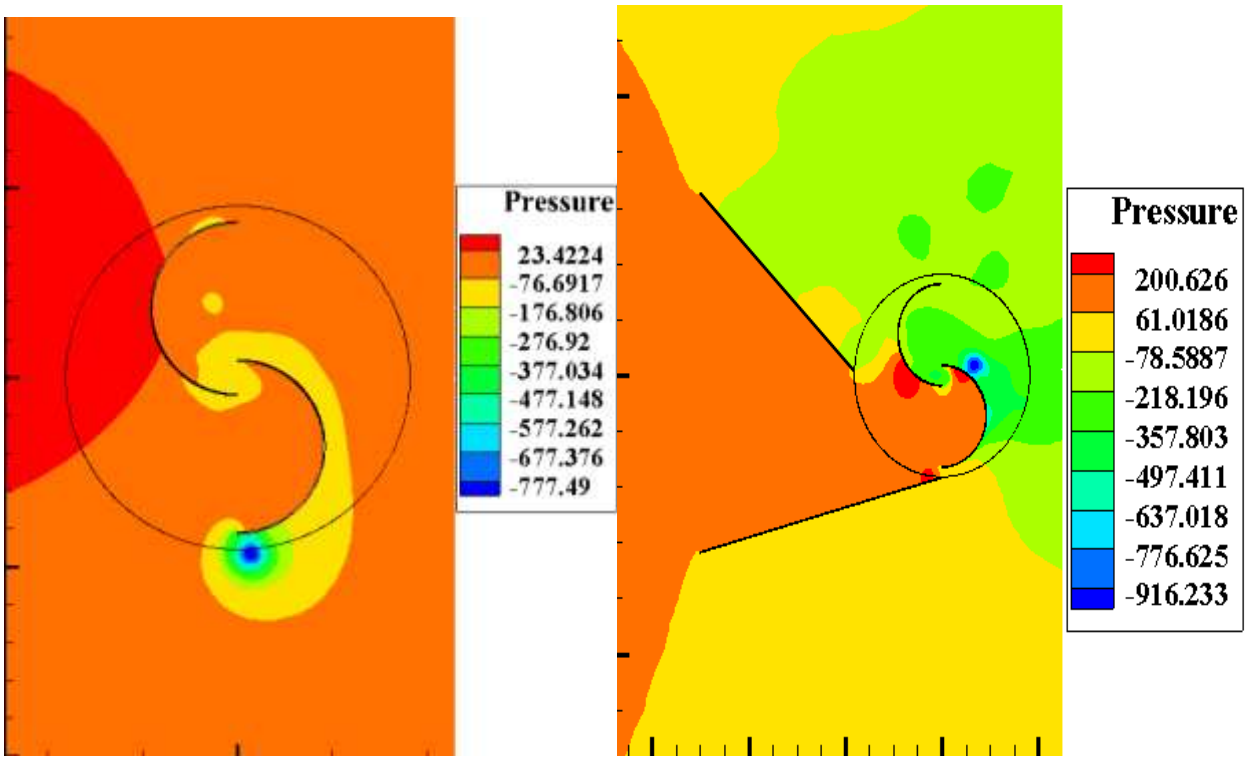

Figure 4.14: Pressure contours comparison between conventional rotor and conventional rotor with curtain plates

For both rotors, the specified pressure is higher at the upstream of the rotor. Later it begins to decrease behind the rotor, which induces pressure difference. At this instant, energy is generated as a result of pressure difference. Low pressure zone is shifted towards the tip of the advancing blade (Convex side) near the overlap region. By using curtain plates, extensive low pressure is created behind the rotor. At the upper plate which acts as a deflector, the pressure intensity is

lower. While besides the lower plate which acts as a concentrator, the pressure magnitude is greater than the upper plate. The maximum value of pressure at upstream of the un-curtain rotor is 23pa. Whereas the maximum value of pressure at upstream of the rotor with curtain is 200pa. The curtain plates around the rotor increase the inlet pressure on the advancing blade of the rotor. While the back pressure on rotor blades decreases. Thus, the pressure drop through the rotor is increased.

The same configuration and design of curtain plates are applied to both i.e. conventional savonius rotor and S1048 section rotor. Some of the basic relationships we got from the above analysis are.

1. The pressure at the upstream is higher than the pressure at the downstream.
2. Behind curtain plates, the pressure is dropped.
3. The line graph is generated between pressure and x-axis of the domain as shown below in Figure 4.15. X-axis includes upstream, rotor area and downstream of the domain.

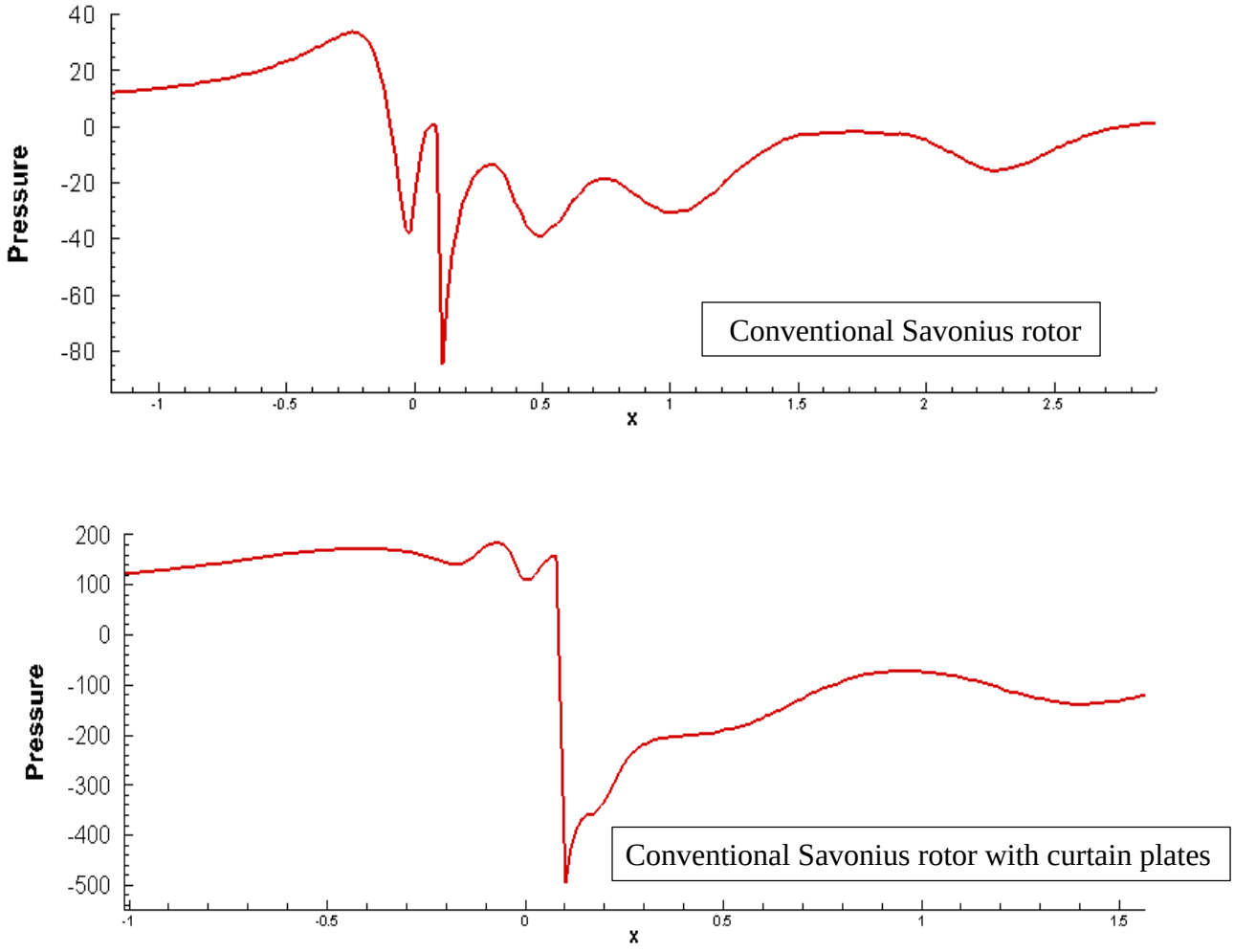

Figure 4.15: Pressure variation along x-axis of domain

From the above plot, we can analyze that pressure drop is maximum in the case of conventional rotor with curtain plates. In conventional rotor without curtain plates the maximum pressure at upstream of the rotor is 38pa. Conversely, the maximum pressure at upstream of conventional rotor with curtain plates is around 140pa. The pressure at downstream of a rotor for conventional savonius rotor and conventional savonius rotor with curtain plates are -20Pa and -150Pa respectively.

Now we will compare the pressure contours of conventional savonius rotor with curtain and S1048 section rotor with curtain plates.

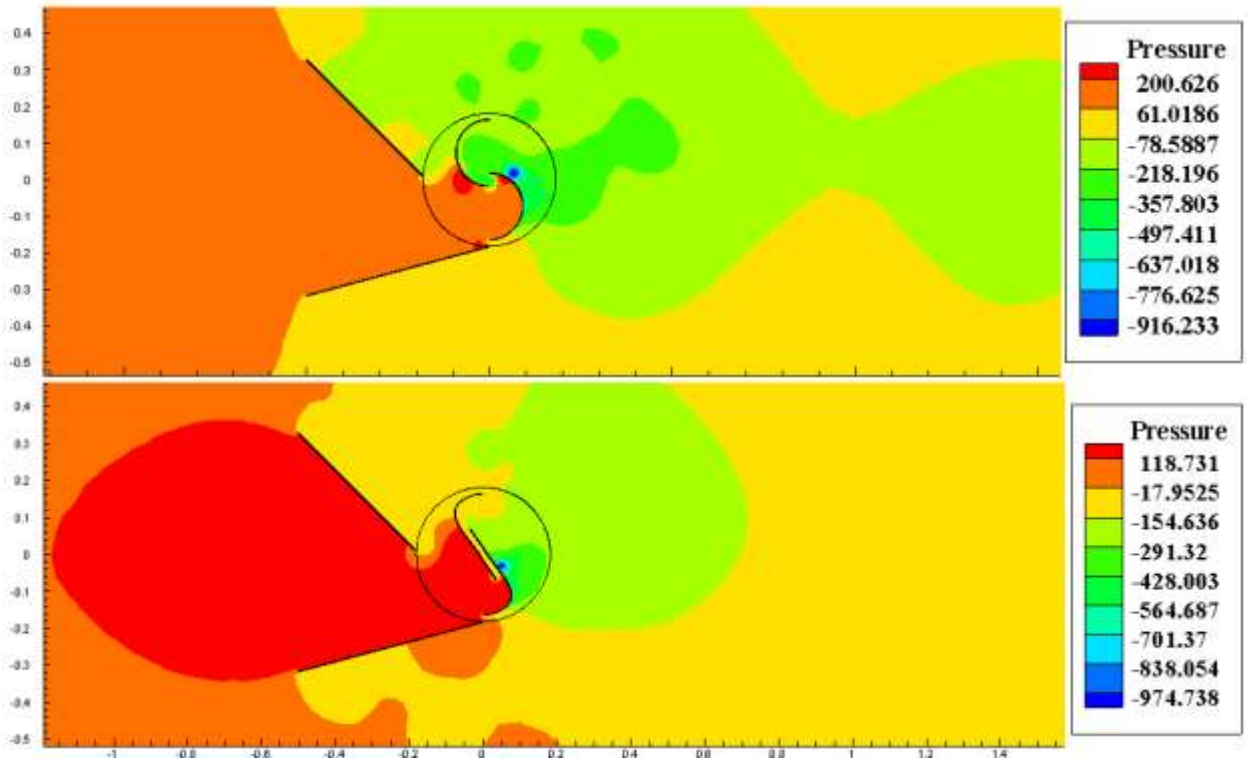

Figure 4.16: Pressure contours of conventional rotor with curtain and S1048 section rotor with curtain

The above contours show that the S1048 section rotor with curtain plates has lesser values of low pressure zone as compared to conventional rotor with curtain plates. The maximum value of pressure in the upstream region of S1048 section rotor with curtain plates is greater than conventional rotor with curtain plates. However at downstream of the rotor, the pressure in the case of S1048 rotor is lesser than conventional rotor which shows that pressure drop in the case of S1048 rotor is greater. Therefore its power coefficient is greater.

4.2.3 Velocity Characteristics

The velocity contours of the un-curtain rotor and rotor with curtain are shown below in Figure 4.17.

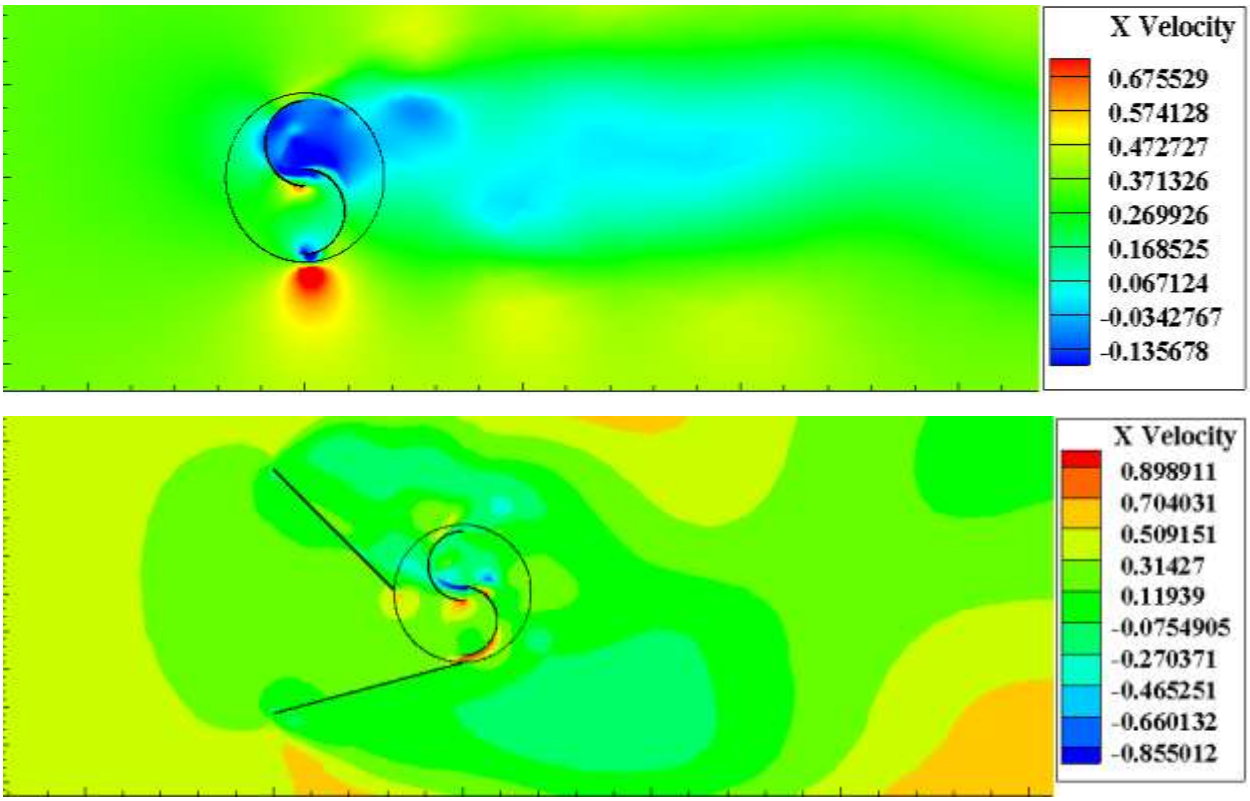

Figure 4.17: Velocity contours comparison between conventional rotor and conventional rotor with curtain plates

The maximum velocity in the case of conventional rotor with curtain plates is 0.89m/s. While for a simple rotor without curtain plates the maximum velocity is 0.67m/s. Moreover, the low speed zones decrease in the rotor with curtain plates. Besides curtain plates, low speed region occurs. Maximum speed zones are obtained near the tip of advancing blades close to the downward curtain plate.

Now we will compare the velocity variation of conventional savonius rotor with curtain and S1048 section rotor with curtain plates. Velocity contours of both cases are shown below.

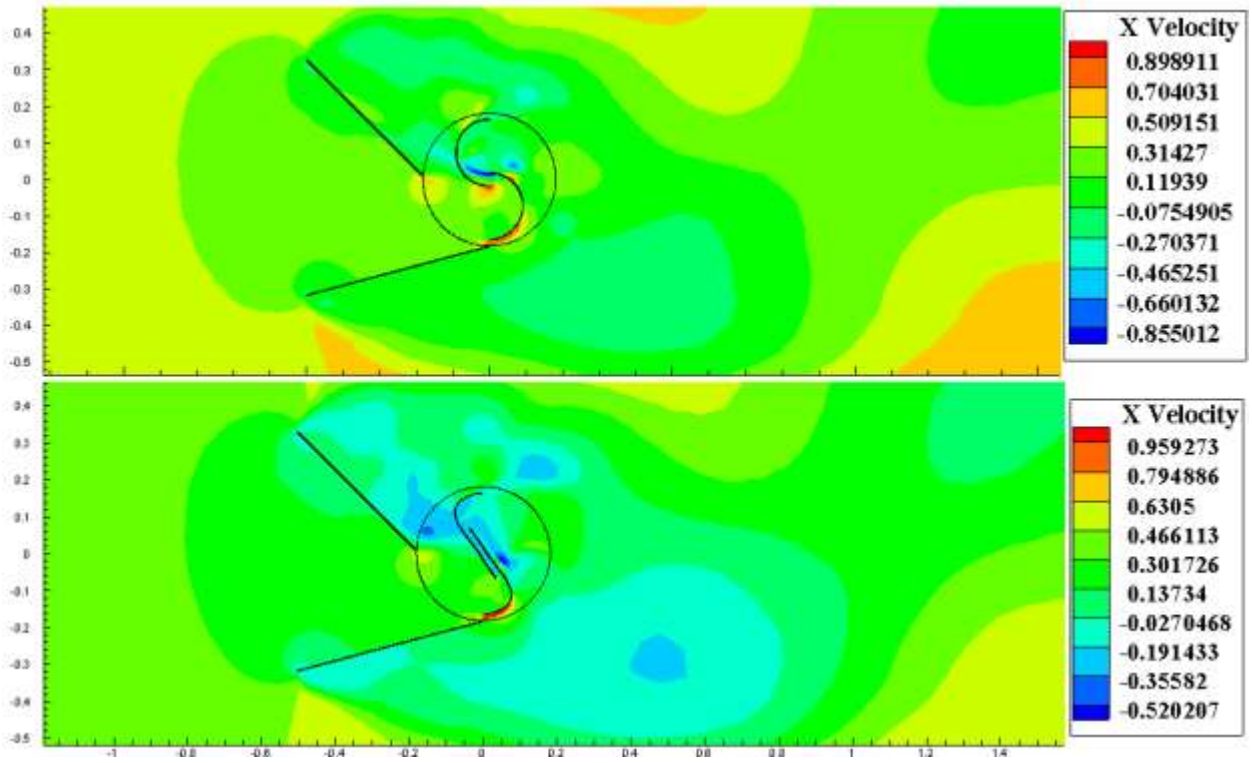

Figure 4.18: Velocity contours of conventional rotor with curtain plates and S1048 section rotor with curtain plates

The maximum velocity of proposed rotor with curtain plates and conventional rotor with curtain plates is 0.95m/s and 0.89m/s respectively. At upstream of the domain, velocity is equal to the inlet velocity which is 0.38m/s. In the rotating domain the velocity at advancing blade increases and reaches to the maximum. The high-speed zone is obtained on the convex side of advancing blades in both cases. Moreover, the minimum velocity for proposed rotor with curtain plates and conventional rotor with curtain plates are -0.52m/s and -0.85m/s respectively.

CHAPTER 5: CONCLUSION AND FUTURE WORK

5.1 Conclusion

The present study is divided into two parts. We will discuss the findings of both parts one by one. In the first part of the study, a novel S1048 profile savonius hydrokinetic turbine is suggested to improve the performance of the rotor. The shape of the blade is generated from the points of S1048 airfoil. A numerical study has been carried out using CFD at an inlet velocity of 0.38m/s for all simulations. The CFD results are verified and compared with the experimental findings of Hayashi [32]. The outcomes of this novel savonius rotor are summarized as follows:

- The maximum power coefficient of S1048 section rotor is 14% higher than conventional savonius rotor at a low water speed of 0.38m/s.
- The S1048 section rotor has a maximum value of power coefficient 0.148 at a tip speed ratio of 1 for low water velocity of 0.38m/s.
- The instantaneous torque coefficient (C_m) tends to increase at the rotor angle 150^o and 305^o.
- At all tip speed ratios, the S1048 section rotor is superior to the conventional savonius rotor in terms of power coefficient.
- The power coefficient of S1048 section rotor is increased due to high speed tip vortices.
- The novel S1048 section rotor provides an additional pressure drop in the domain, which in return increases the speed and performance of the rotor.

The second part of the study includes the performance enhancement of the rotor using a suitable augmentation system. The optimal curtain arrangement which is tested and analyzed by Altan [7] is used in this section. The geometry and parameters of curtain plates are selected from the optimal design of Altan [7]. This curtain arrangement has two plates placed at the upstream of the rotor. The upper plate reduces the negative torque produced by the returning blade while the lower plate concentrates the fluid towards the advancing blade. The outcomes of this part of the research are summarized as follows:

- By using a curtain arrangement the maximum power coefficient of conventional savonius rotor is increased from 0.128 to 0.38.

- The pressure drop in the case of curtain plates is higher than without curtain plates.
- The maximum power coefficient of S1048 section rotor with curtain plates is 0.43, which 13% greater than the conventional savonius rotor with curtain plates at a tip speed ratio of 1.
- The velocity of water is increased to 1.49m/s and 1.74m/s for conventional rotor and S1048 section rotor respectively using curtain plates.
- The S1048 section rotor with curtain plates shows a greater pressure drop in the stationary domain than conventional rotor with curtain plates. Hence proposed savonius rotor with curtain plates has a higher power coefficient than conventional rotor with curtain plates.

5.2 Future work:

For future work, a full scale model of proposed rotor (S1048 section rotor) could be manufactured and tested experimentally in a water tunnel. The novel augmentation system could be designed and analyzed numerically to enhance the performance of the rotor. Moreover, the overlap ratio between the blades can be varied and its flow characteristics can be investigated. In addition, a twist angle and aspect ratio can also be varied to acquire optimum performance. According to literature review, the performance of savonius rotor can also be increased with the addition of end plates. The performance of proposed savonius rotor can also be improved by the blend of optimization algorithms i.e. surface response and particle swarm techniques. 3D analysis can be carried out. Moreover, high fidelity CFD simulation like hybrid RANS-LES and LES could be used for more insight into and modification of the proposed design.

REFERENCES

[1] K. A. K Kaygusuz, 'Renewable energy and sustainable development in Turkey', *Renew. Energy*, vol. 25:431–53, 2002.

[2] S. Ashok, 'Optimised model for community-based hybrid energy system', *Renew. energy*, vol. 32, no. 7, pp. 1155–1164, 2007.

[3] T. Hoq, U. A. Nawshad, N. Islam, K. Syfullah, and R. Rahman, 'Micro hydro power: promising solution for off-grid renewable energy source', *Int. J. Sci. Eng. Res*, vol. 2, no. 12, pp. 2–6, 2011.

[4] M. J. Khan, G. Bhuyan, M. T. Iqbal, and J. E. Quaicoe, 'Hydrokinetic energy conversion systems and assessment of horizontal and vertical axis turbines for river and tidal applications: A technology status review', *Applied Energy*. 2009.

[5] M. S. Güney and K. Kaygusuz, 'Hydrokinetic energy conversion systems: A technology status review', *Renewable and Sustainable Energy Reviews*. 2010.

[6] P. Garman, 'Water current turbines: providing pumping, power in remote areas', *Hydro Rev. Worldw.*, vol. 6, no. 5, pp. 24–28, 1998.

[7] B. D. Altan, M. Atılgan, and A. Özdamar, 'An experimental study on improvement of a Savonius rotor performance with curtaining', *Exp. Therm. fluid Sci.*, vol. 32, no. 8, pp. 1673–1678, 2008.

[8] K. S. Jeon, J. I. Jeong, J.-K. Pan, and K.-W. Ryu, 'Effects of end plates with various shapes and sizes on helical Savonius wind turbines', *Renew. energy*, vol. 79, pp. 167–176, 2015.

[9] S. Sivasegaram, 'Secondary parameters affecting the performance of resistance-type vertical-axis wind rotors', *Wind Eng.*, pp. 49–58, 1978.

[10] A. Kumar and R. P. Saini, 'Performance parameters of Savonius type hydrokinetic turbine–A Review', *Renew. Sustain. Energy Rev.*, vol. 64, pp. 289–310, 2016.

[11] N. H. Mahmoud, A. A. El-Haroun, E. Wahba, and M. H. Nasef, 'An experimental study on improvement of Savonius rotor performance', *Alexandria Eng. J.*, vol. 51, no. 1, pp. 19–25, 2012.

[12] R. E. Sheldahl, B. F. Blackwell, and L. V Feltz, 'Wind tunnel performance data for two-and three-bucket Savonius rotors', *J. Energy*, vol. 2, no. 3, pp. 160–164, 1978.

[13] S. Roy and U. K. Saha, 'Wind tunnel experiments of a newly developed two-bladed

Savonius-style wind turbine', *Appl. Energy*, vol. 137, pp. 117–125, 2015.

[14] L. Chen, J. Chen, and Z. Zhang, 'Review of the Savonius rotor's blade profile and its performance', *J. Renew. Sustain. Energy*, vol. 10, no. 1, p. 13306, 2018.

[15] N. Alom and U. K. Saha, 'Four decades of research into the augmentation techniques of Savonius wind turbine rotor', *J. Energy Resour. Technol.*, vol. 140, no. 5, 2018.

[16] M. Nakajima, S. Iio, and T. Ikeda, 'Performance of Savonius rotor for environmentally friendly hydraulic turbine', *J. Fluid Sci. Technol.*, vol. 3, no. 3, pp. 420–429, 2008.

[17] M. Khan, N. Islam, T. Iqbal, M. Hinchey, and V. Masek, 'Performance of Savonius rotor as a water current turbine', *J. Ocean Technol.*, vol. 4, no. 2, pp. 71–83, 2009.

[18] G. Kailash, T. I. Eldho, and S. V Prabhu, 'Performance study of modified Savonius water turbine with two deflector plates', *Int. J. Rotating Mach.*, vol. 2012, 2012.

[19] V. Patel, G. Bhat, T. I. Eldho, and S. V Prabhu, 'Influence of overlap ratio and aspect ratio on the performance of Savonius hydrokinetic turbine', *Int. J. Energy Res.*, vol. 41, no. 6, pp. 829–844, 2017.

[20] O. Yaakob, Y. M. Ahmed, and M. A. Ismail, 'Validation study for Savonius vertical axis marine current turbine using CFD simulation', in *The 6th Asia-Pacific Workshop on Marine Hydrodynamics-APHydro2012*, 2012, pp. 3–4.

[21] N. K. Sarma, A. Biswas, and R. D. Misra, 'Experimental and computational evaluation of Savonius hydrokinetic turbine for low velocity condition with comparison to Savonius wind turbine at the same input power', *Energy Convers. Manag.*, vol. 83, pp. 88–98, 2014.

[22] A. Kumar and R. P. Saini, 'Performance analysis of a Savonius hydrokinetic turbine having twisted blades', *Renew. Energy*, vol. 108, pp. 502–522, 2017.

[23] A. H. Elbatran, Y. M. Ahmed, and A. S. Shehata, 'Performance study of ducted nozzle Savonius water turbine, comparison with conventional Savonius turbine', *Energy*, vol. 134, pp. 566–584, 2017.

[24] P. K. Talukdar, A. Sardar, V. Kulkarni, and U. K. Saha, 'Parametric analysis of model Savonius hydrokinetic turbines through experimental and computational investigations', *Energy Convers. Manag.*, vol. 158, pp. 36–49, 2018.

[25] M. Mosbahi, A. Ayadi, Y. Chouaibi, Z. Driss, and T. Tucciarelli, 'Performance study of a Helical Savonius hydrokinetic turbine with a new deflector system design', *Energy Convers. Manag.*, vol. 194, pp. 55–74, 2019.

[26] H. Alizadeh, M. H. Jahangir, and R. Ghasempour, ‘CFD-based improvement of Savonius type hydrokinetic turbine using optimized barrier at the low-speed flows’, *Ocean Eng.*, vol. 202, p. 107178, 2020.

[27] J. D. Riglin, ‘Design, Modeling, and Prototyping of a Hydrokinetic Turbine Unit for River Application’, 2016.

[28] F. R. Menter, ‘Two-equation eddy-viscosity turbulence models for engineering applications’, *AIAA J.*, vol. 32, no. 8, pp. 1598–1605, 1994.

[29] A. Fluent, ‘12.0 Theory Guide’, *Ansys Inc*, 2009.

[30] D. C. Wilcox, *Turbulence modeling for CFD*, vol. 2. DCW industries La Canada, CA, 1998.

[31] I. Paraschivoiu, *Wind turbine design: with emphasis on Darrieus concept*. Presses inter Polytechnique, 2002.

[32] T. Hayashi, Y. Li, and Y. Hara, ‘Wind tunnel tests on a different phase three-stage Savonius rotor’, *JSME Int. J. Ser. B Fluids Therm. Eng.*, vol. 48, no. 1, pp. 9–16, 2005.

[33] A. Sanusi, S. Soeparman, S. Wahyudi, and L. Yuliati, ‘Experimental study of combined blade savonius wind turbine’, *Int. J. Renew. Energy Res.*, vol. 6, no. 2, pp. 614–619, 2016.

[34] K. Rogowski and R. Maroński, ‘CFD computation of the Savonius rotor’, *J. Theor. Appl. Mech.*, vol. 53, no. 1, pp. 37–45, 2015.

[35] B. Yang and C. Lawn, ‘Fluid dynamic performance of a vertical axis turbine for tidal currents’, *Renew. Energy*, vol. 36, no. 12, pp. 3355–3366, 2011.

[36] J. V. Akwa, G. A. da Silva Júnior, and A. P. Petry, ‘Discussion on the verification of the overlap ratio influence on performance coefficients of a Savonius wind rotor using computational fluid dynamics’, *Renew. energy*, vol. 38, no. 1, pp. 141–149, 2012.

[37] M. Mohammadi, R. Mohammadi, A. Ramadan, and M. H. Mohamed, ‘Numerical investigation of performance refinement of a drag wind rotor using flow augmentation and momentum exchange optimization’, *Energy*, vol. 158, pp. 592–606, 2018.

[38] A. Tools, ‘http://www.airfoiltools.com/plotter/index’.

Zain Thesis

ORIGINALITY REPORT

3%	2%	5%	1%
SIMILARITY INDEX	INTERNET SOURCES	PUBLICATIONS	STUDENT PAPERS

PRIMARY SOURCES

1	Anuj Kumar, R.P. Saini. "Performance parameters of Savonius type hydrokinetic turbine – A Review", Renewable and Sustainable Energy Reviews, 2016 Publication	2%
2	Roy, S., and U. K. Saha. "Review of experimental investigations into the design, performance and optimization of the Savonius rotor", Proceedings of the Institution of Mechanical Engineers Part A Journal of Power and Energy, 2013. Publication	1%
3	Anuj Kumar, R.P. Saini. "Performance analysis of a Savonius hydrokinetic turbine having twisted blades", Renewable Energy, 2017 Publication	1%

Exclude quotes	On	Exclude matches	< 1%
Exclude bibliography	On		